Optogenetic control of phosphate-responsive genes using single component fusion proteins in *Saccharomyces cerevisiae*

Matthew M. Cleere[a,b] and Kevin H. Gardner[a,c,d]

[a] Structural Biology Initiative, CUNY Advanced Science Research Center, New York, NY 10031

[b] Biology Ph.D. Program, Graduate Center, City University of New York, New York, NY 10016

[c] Biochemistry, Chemistry, and Biology Ph.D. Programs, Graduate Center, City University of New York, New York, NY 10016

[d] Department of Chemistry and Biochemistry, City College of New York, New York, NY 10031

ORCiD

Matthew M. Cleere - 0000-0003-3285-6949

Kevin H. Gardner - 0000-0002-8671-2556

Keywords

Optogenetics, EL222, LOV domain, chromatin, inorganic phosphate (P_i), yeast, transcription

ABSTRACT

Blue light illumination can be detected by Light-Oxygen-Voltage (LOV) photosensing proteins and translated into a range of biochemical responses, facilitating the generation of novel optogenetic tools to control cellular function. Here, we develop new variants of our previously described VP-EL222 light-dependent transcription factor and apply them to study the phosphate-responsive signaling (*PHO*) pathway in the budding yeast *Saccharomyces cerevisiae*, exemplifying the utilities of these new tools. Focusing first on the VP-EL222 protein itself, we quantified the tunability of gene expression as a function of light intensity and duration, and demonstrated that this system can tolerate the addition of substantially larger effector domains without impacting function. We further demonstrated the utility of several EL222-driven transcriptional controllers in both plasmid and genomic settings, using the *PHO5* and *PHO84* promoters in their native chromosomal contexts as examples. These studies highlight the utility of light-controlled gene activation using EL222 tethered to either artificial transcription domains or yeast activator proteins (Pho4). Similarly, we demonstrate the ability to optogenetically repress gene expression with EL222 fused to the yeast Ume6 protein. We finally investigated the effects of moving EL222 recruitment sites to different locations within the *PHO5* and *PHO84* promoters, as well as determining how this artificial light-controlled regulation could be integrated with the native controls dependent on inorganic phosphate (P_i) availability. Taken together, our work expands the applicability of these versatile optogenetic tools in the types of functionalities they can deliver and biological questions that can be probed.

INTRODUCTION

Light is a ubiquitous environmental stimulus, harnessed by diverse organisms to control wide-ranging biological responses via photosensory proteins. Such proteins absorb light, triggering photochemical events at an internally-bound chromophore that are subsequently converted into conformational changes in the surrounding protein, culminating in altered downstream biological responses[4].

In their simplest implementations, photosensors consist of two domains – a sensory domain and an effector – as exemplified by EL222, a 222-residue light-regulated transcription factor found in the marine bacterium *Erythrobacter litoralis HTCC2594*[5, 6]. The EL222 sensory component is a Light-Oxygen-Voltage (LOV) domain, a photosensory subset of the Per-ARNT-Sim (or PAS) superfamily of sensory proteins[7, 8], which senses blue light via an internally-bound flavin chromophore. In addition, EL222 contains a single effector domain, a Helix-Turn-Helix (HTH) DNA binding domain. In the dark state, this protein adopts a "closed" monomeric structure, unable to bind DNA due to steric clashes preventing an obligate protein dimerization step. Upon blue light exposure, the flavin chromophore undergoes a photochemical reduction and concomitant adduct formation with a nearby cysteine residue, opening EL222 into a conformation exposing dimerizing surfaces in both the LOV and HTH domains, promoting DNA binding as a dimer[5, 9].

Given its simplicity, reversible photoactivation, and rapid activation/deactivation kinetics, EL222 has been widely used as an optogenetic tool for transcriptional control in prokaryotes and eukaryotes[10-15]. In its original construction for eukaryotic applications, the first 13 residues of EL222 were replaced with a Nuclear Localization Sequence (NLS) and a VP16 Transcription Activation Domain (TAD), enabling "VP-EL222" to enter the nucleus and upon DNA binding, recruit RNA polymerase II to initiate transcription[10]. Parallel optimization of DNA binding sites by a combination of genomic mapping, SELEX (Systematic Evolution of Ligands by EXponential enrichment)[16], and *in vitro* optimization led to the identification of a high affinity, non-native 20 bp

binding sequence named "C120". By arranging a five-fold tandem arrangement of this sequence (5xC120) in front of a minimal TATA promoter, we generated a potent and tunable system for increased gene expression under light activation[10]. Since this initial characterization, VP-EL222 has been used to control gene expression in multiple host systems including the budding yeast *Saccharomyces cerevisiae*[10, 11, 17, 18], with the versatility provided by its precision tunability enabling investigations of diverse biological functions (e.g. characterization of fluorescent protein maturation) and new biotech applications via light-controlled expression of enzymes needed for microbial chemical production[17, 19, 20].

Complementing this work with an artificial light-controlled promoter, *S. cerevisiae* has long been a workhorse for studies characterizing naturally-inducible promoters, as exemplified by the *PHO5* promoter[21], a model for understanding how epigenetic control of gene transcription harnesses chromatin organization to differentially occlude cofactor binding sites[22]. *PHO5*, as well as the inorganic phosphate (P_i) transmembrane transporter gene *PHO84*, is part of the larger phosphate-responsive signaling (PHO) pathway or *PHO* regulon that mediates the yeast phosphate stress response[23]. When phosphate is abundant, the promoter regions of *PHO5* and *PHO84* are nucleosome-bound[1], blocking transcription factors such as Pho4 from accessing critical Upstream Activation Sequences (UAS) and the TATA box[2, 3]. As phosphate is depleted, dephosphorylated Pho4 (joined by Pho2) binds to a specific UAS, recruiting the SAGA (Spt-Ada-Gcn5 Acetyltransferase) complex to hyperacetylate histones in nearby nucleosomes[24-26], causing them to unwind and reveal the previously-occluded binding sequences[1, 2, 25, 27, 28]. With these sites now accessible, transcription factors bind and drive expression of the *PHO5* and *PHO84* genes.

While conventional approaches have successfully characterized many aspects of *PHO5* and *PHO84* regulation, they have been unable to tackle certain questions due to fundamental limitations in existing tools. We believe that having access to reagents that can dynamically and precisely control gene expression are critical for fully manipulating transcriptional circuitry such

as this, leading us to explore the versatility of VP-EL222 variants to better understand the nature of these chromatin driven promoters. In *S. cerevisiae*, some of the major complexes involved in chromatin remodeling and gene activation are SAGA (histone acetylation) and Rpd3S or Rpd3L (histone deacetylation). When SAGA is recruited to DNA by transcriptional activators such as Pho4, it binds and acetylates the histone tails of nearby nucleosomes through the Gcn5 histone acetyltransferase catalytic domain[29-31], using acetyl-CoA for acetylation produced by the yeast acetyl-CoA synthetase ACS2 as a substrate[32-34]. For gene repression, the DNA-binding transcriptional regular Ume6 recruits Rpd3 histone deacetylation complexes to remove acetyl marks from nearby nucleosomes[22, 35, 36].

In light of the roles of these diverse proteins and complexes in controlling gene expression, we pondered whether their light-dependent recruitment via EL222 could lead to a powerful new group of optogenetic transcriptional regulatory reagents. Here we report our first steps in developing such EL222 fusion constructs with a range of catalytic and non-catalytic components installed as N-terminal fusions to EL222's LOV-HTH core. These effectors included catalytic domains involved in gene activation through chromatin regulation (Gcn5, Acs2, and Rpd3) as well as factors which recruit coactivator (Pho4) or corepressor (Ume6) complexes. We characterized the performance of these optogenetic regulators in *S. cerevisiae* in both plasmid-based and genomic settings, providing insights to the broader utility of these fusion proteins for probing two promoter regions of the yeast *PHO* regulon. Notably, EL222 variants containing Pho4 or Ume6 successfully activated and repressed target genes in predictable ways dependent on environmental factors (e.g. light, P_i concentration) and proximity to transcriptional start sites, demonstrating the utility of EL222-based approaches for up or downregulating targets in genomic contexts.

RESULTS

Tunability of EL222 in yeast using a single reporter plasmid

Our previously-published VP-EL222 optogenetic tool construct consists of NLS and VP16 sequences fused N-terminal to a truncated EL222 fragment (residues 14-222) which binds to the non-native, high affinity C120 sequence upon illumination (Figure S1a)[10, 16]. C120 can be arranged in a five-fold tandem repeat (5xC120) in front of a minimal TATA promoter for increased gene expression under light activation (Figure 1a). To investigate the temporal

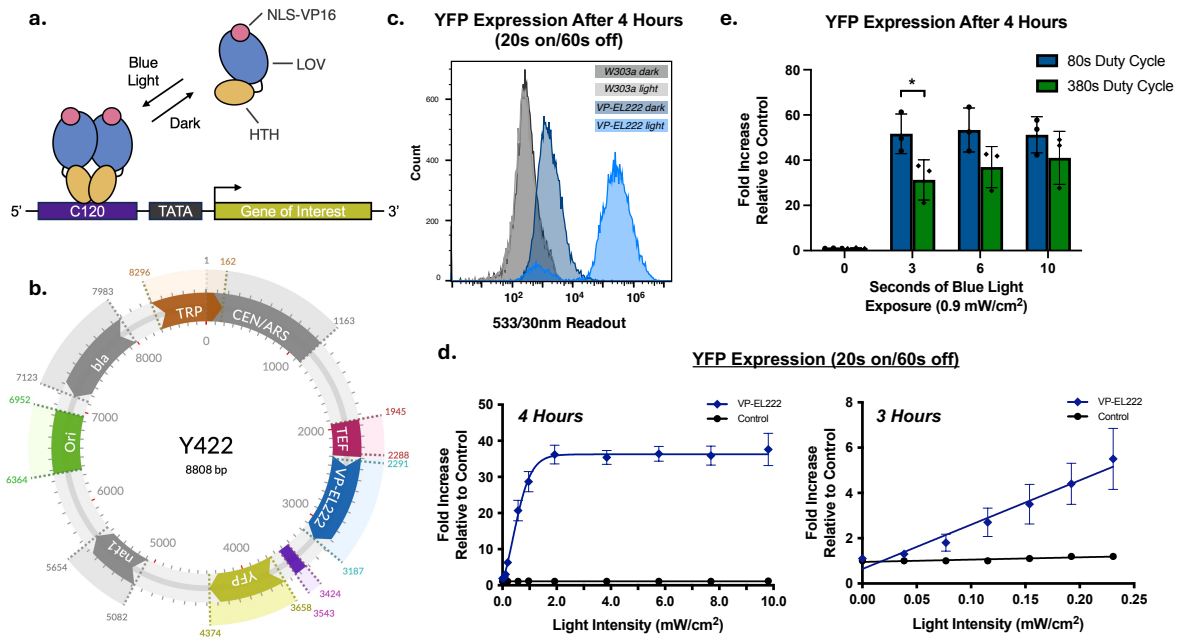

Figure 1. Plasmid-based expression of VP-EL222 driving Yellow Fluorescent Protein (YFP) production in *S. cerevisiae*. (a) Model of the blue-light activated transcription factor EL222 engineered for eukaryotic expression through addition of an N-terminal Nuclear Localization Sequence (NLS) and VP16 Transcription Activation Domain (TAD). In the dark, VP-EL222 is unable to bind DNA. Upon activation with blue light, VP-EL222 binds to the non-native C120 sequence (repeated five times), driving transcription of a downstream Gene of Interest (GOI). (b) Map of the yeast centromeric plasmid Y422 consisting of a constitutively active VP-EL222 (blue) driven by an *A. gossypii* TEF promoter (maroon), 5xC120 binding sequences (purple), YFP (yellow), origin of replication (green), tryptophan auxotrophic marker (brown), antibiotic resistance markers beta-lactamase and nourseothricin (gray), and the *S. cerevisiae* CEN4 centromere fused to the autonomously replicating sequence ARS1 (gray). (c) Flow cytometry histogram of W303a wildtype and Y422 transformed cells showing YFP activity in the dark and light after 4 hours (20 s on at 0.9 mW/cm^2, 60 s off). (d) Tunable VP-EL222 activity reflected by YFP expression after blue light exposure (20 s on/60 s off). (e) VP-EL222 activity based on duty cycle variations (seconds of blue light exposure within a total cycle length outlined in the figure key). Data shown are mean ± SD. Significance was calculated using Two-Way ANOVA with Turkey's multiple comparison test. *$p \leq 0.05$.

flexibility of VP-EL222 under various conditions, the Y422 yeast centromeric plasmid was developed for expression in *S. cerevisiae* under tryptophan deficient auxotrophic selection. This system utilizes VP-EL222 constitutively expressed by the *Ashbya gossypii* TEF fungal promoter, generating protein which binds elsewhere in the plasmid at the 5xC120 sequence upon blue light illumination, driving production of a yeast-optimized Yellow Fluorescent Protein (YFP) to quantitate EL222 activity (Figure 1b).

To test the efficiency of this system, we used flow cytometry in the 533/30nm FITC channel to probe for YFP expression. As expected, *S. cerevisiae* W303a cells registered no change in fluorescence activity upon blue light activation, confirming that they are a suitable background for optogenetic testing. After transformation with the Y422 plasmid, we observed a minimal (~5%) leakiness of VP-EL222 activity, consistent with our past experience[10] and many other optogenetic systems[37]. After 4 hours of pulsed blue light cycles (20 s on at 0.9 mW/cm^2, 60 s off), we saw a >100-fold increase in VP-EL222 driven YFP activity (Figure 1c; gating approaches Figure S2). Similar results were seen with a plate reader-based readout, with YFP expression increased 30-fold (Figure 1d).

We quantified the intensity dependence of VP-EL222 driven gene expression in *S. cerevisiae* with a programable, in-house 96-well LED apparatus and titrating a gradient of light across each plate of cells (20 s on/60 s off). Using an 8-bit Arduino UNO microcontroller, we programmed each LED (with a λ_{peak} of 464.7 nm) from 0-255 intensity steps of 0.036 mW/cm^2 each (Figure S3a-d). As light intensity strengthened, YFP expression increased until hitting 1.8 mW/cm^2, where it registered a ~36 fold increase relative to control after 4 hours. From there, YFP expression remained invariant to additional illumination, up to a maximum intensity of 9.2 mW/cm^2. To develop a one-for-one relationship of light intensity to fold increase, we reduced both the total assay duration to 3 hours and focused on the lowest settings in the system. At the minimum intensities of ~0.04-0.24 mW/cm^2, a near linear pattern emerged (Figure 1d).

To understand the flexibility of time within each duty cycle, we explored both seconds of blue light exposure as well as length of intermittent darkness, keeping in mind the approximate 30 s time for the spontaneous reversion of EL222/chromophore structure and VP-EL222 driven gene expression we observed in mammalian cells[5, 10]. Within our standard 80 s total cycle (20 s on/60 s off), shortening the illumination periods down to 10, 6, and 3 seconds (with corresponding lengthening of the dark periods) produced no discernable change. However, when we extended the total cycle duration from 80 s to 380 s, we began to see corresponding reduction of YFP expression, consistent with the dark deactivation time being substantially shorter than these longer dark periods. This became statistically significant at 3 s on/377 s off when compared to the 80 second cycles (Figure 1e). Further tests were performed to see the impact of light intensity when the total number of photons exposed to VP-EL222 remained the same. Short bursts of high intensity light outperformed extended periods of low light intensity, even in extended off cycles (Figure S4a-c). When we looked at the strength of single 60 s exposures, we observed a jump in YFP expression at the saturation point of 1.8 mW/cm^2 out to 4 hours post-illumination (Figure S4d).

Exploring the generality of EL222 fusions for light-dependent DNA recruitment

Compared to two-component systems, such as light-driven two-hybrid like associations of separated DNA binding and TAD activities, single protein systems like VP-EL222 are often easier to optimize and exhibit fewer technical drawbacks[4, 38]. However, a key variable of EL222-driven tools – their ability to tolerate fusions of molecular cargoes large than simple TADs – has not yet been rigorously tested to the best of our knowledge. To probe these constraints, we inserted a 26.7 kDa mCherry protein between the N-terminal NLS and TAD sequences and the LOV-HTH core in the Y422 background, letting us both examine the impact of this larger cargo on VP-EL222 function and enable the independent measurement of EL222 levels and activity via mCherry and YFP-selective fluorescence monitoring, respectively. Of note, we found that a

substantial spacer between mCherry and the LOV-HTH core was essential for function, settling on a $(GGGGS)_9$ linker in our final construct (Figure S1a). With this fusion protein in the reporter assays outlined in Figure 1 with a 20 s on/60 s off cycle for 4 hours at varying light intensities, we saw robust YFP production, indicating that photoreceptor function was unperturbed with the addition of this large protein. Additionally, our simultaneous observation of mCherry fluorescence provided strong evidence that exogenous domains can still properly fold and function while tethered to EL222.

To directly compare the performance of VP-mCherry-EL222 and VP-EL222 tools, we performed the optogenetic reporter assay at a light intensity of 3.6 mW/cm^2 and saw comparable YFP expression to VP-EL222 with the 298 aa VP-EL222 and 595 aa VP-mCherry-EL222 demonstrating 43- and 44-fold increases using the plate reader, respectively (Figure 2a). Using widefield microscopy, we observed VP-mCherry-EL222 driven YFP production within the nuclei and cytosols of yeast cells. We also observed high levels of intracellular mCherry fluorescence, indicating proper functionality of this fluorescent protein (Figures 2b and S5). DAPI stained nuclei can be seen in the blue channel with their positions related to cellular fluorescence apparent when merged (Figure 2b).

We wanted to test the limits of our fusion constructs by replacing mCherry with effector domains we planned to utilize *in vivo*. The largest of these sequences was ACS2 (683 residues), substantially larger than mCherry and resulting in a 1,029 residue (111.2 kDa) VP-Acs2-EL222 complete fusion (Figure S1a). As with the smaller mCherry-containing construct, the inclusion of these large effector domains minimally impacted optogenetic gene expression, with VP-mCherry-EL222 producing a 117-fold increase in YFP expression versus a 75-fold increase for VP-Acs2-EL222 in a 4 hour fluorescence analyzer assay (Figure 2c; Figure S6b). Similar activity was also seen in the 784 residue VP-Gcn5-EL222 construct (Figure S6d). In contrast, we were unsuccessful in generating active VP-mCherry-Acs2-EL222 and VP-mCherry-Gcn5-EL222 constructs that exceeded the single domain-linker model, as no YFP expression or

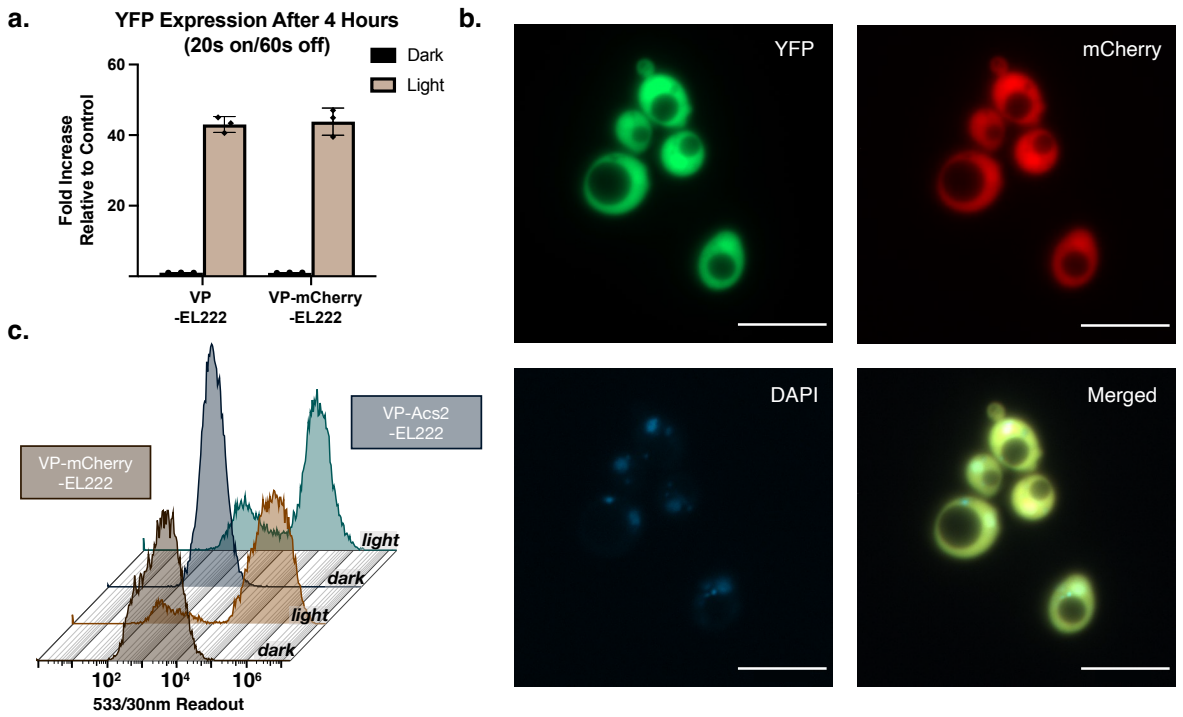

Figure 2. Relative activity of VP-EL222 fusion constructs with additional domains attached to the N-terminus of the LOV core through a flexible linker. (a) YFP activity of VP-EL222 and VP-mCherry-EL222 constructs after 4 hours (20 s on/60 s off) with a light intensity of 3.6 mW/cm^2. (b) Wide-field microscope images of *Saccharomyces cerevisiae* cells displaying YFP production in the GFP channel (top left), mCherry activity (top right), DAPI staining of nuclei (bottom left), and merged layers (bottom right). *Scale bar = 10 μM*. (c) Flow cytometry histogram waterfall plots of VP-mCherry-EL222 and VP-Acs2-EL222 after 4 hours (20 s on/60 s off) with a light intensity of 0.9 mW/cm^2.

mCherry activity were observed with these systems (Figures S6c, e).

Targeting yeast acid phosphatase genes using CRISPR and EL222 fusion constructs

With these optogenetic tools in hand, we proceeded to test them in genomic contexts starting with the *PHO5* gene, which encodes an enzyme responsible for phosphate hydrolysis important for cellular responses during periods of phosphate starvation[39]. Under high phosphate conditions (>300 μM), histones are tightly wrapped around the *PHO5* promoter region, obstructing both the TATA box and one of the two Upstream Activation Sequences (UAS)[1, 40]. This blocks the binding of the Pho4 transcription factor binds to the UAS, with an additional layer of repression caused by hyperphosphorylation-induced sequestration to the cytosol. As phosphate is depleted, Pho4 slowly dephosphorylates and becomes nuclear. Eventually, Pho4

can bind one of the two UAS (UASp1) (in association with Pho2) and recruit the SAGA complex to hyperacetylate surrounding histones[24-26]. These nucleosomes begin to unwind until the histones are ejected, exposing the second UAS site (UASp2) and TATA box. In this state, Pho4 binds UASp2 and induces transcription of *PHO5*[1, 25, 41-43].

While *PHO5* responses to phosphate starvation are based on phosphatase production, a parallel response involves the upregulation of P_i transmembrane transporters encoded by the gene *PHO84*[44]. Like *PHO5*, *PHO84* is dependent on the transactivator Pho4 for activation, via a promoter that consists of 5 upstream activation sequences (UASpA-E) where UASpC/D act as high affinity sites with UASpB and UASpE occluded by upstream and downstream nucleosomes[2]. Upon phosphate depletion, these nucleosomes are ejected and *PHO84* transcription is induced (Figure 3a)[1]. However, it is important to note that *PHO5* and *PHO84* exhibit very different induction profiles with depleting levels of phosphate. As concentrations of inorganic phosphate (P_i) are incrementally dropped from 250 μM to 0, *PHO84* undergoes a graded transition to activation where *PHO5* is more binary, staying nearly inactive until full depletion occurs[42].

To probe these genes with our newly-developed EL222 tools, we utilized CRISPR technology to stably integrate the 5xC120 binding sequence into the yeast genome (Figure S7). Then, we re-engineered the Y422 plasmid through our validations in Figure 2 into a plug-and-go construct named "Y423" for transient expression in the 5xC120 integrated background cells. For the Y423 constructs, the 5xC120 and YFP reporter sequences have been removed completely. Additionally, we replaced the VP16 TAD with a flexible linker engineered to facilitate fusing any effectors of our choice into the plasmid with standard restriction enzyme approaches (Figure 3b). Two of the catalytic domain constructs were tested in the Y422 plasmid background (20 s on at 0.9 mW/cm^2, 60 s off) to confirm these effectors did not induce changes in gene expression through Pol II recruitment alone, and after 4 hours had produced no YFP activity in

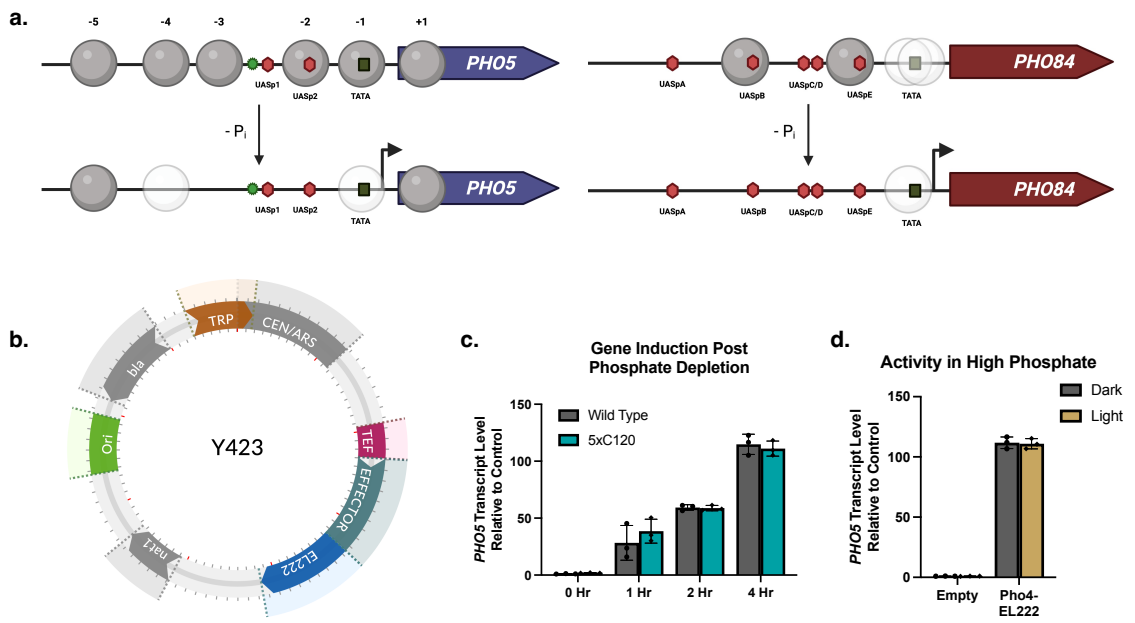

Figure 3. Induction of the yeast acid phosphatase genes *PHO5* and *PHO84* under native and non-native conditions. (a) In a high phosphate environment, some of the Upstream Activating Sequences (red hexagons) in the *PHO5* and *PHO84* promoters are blocked through steric occlusion by nucleosome forming histones. As inorganic phosphate (P_i) is depleted, transcription factors such as Pho4 bind to the available UASp's and initiate chromatin remodeling, leading to the eventual ejection of multiple histones and exposure of new UASp's. More factors bind to these sequences eventually driving transcription of the *PHO5* and *PHO84* genes[1-3]. Dark spheres represent clearly positioned histones while faded spheres represent less organized nucleosomes. The green star indicates the initial insertion point of the 5xC120 binding sequence adjacent *PHO5*'s UASp1 site using CRISPR. (b) Generic map of the Y423 plasmids generated from the original Y422 plasmid. New effector domains are N-terminally fused to the LOV core through a flexible linker and the 5xC120-YFP reporter sequence has been removed. (c) Comparison of *PHO5* gene induction after phosphate depletion over 4 hours in both W303a wild type and 5xC120 promoter integrated cells. (d) Dark and light *PHO5* gene activity in high phosphate for the Pho4-EL222 construct and "Empty" NLS-EL222 control after 4 hours (20 s on at 15 mW/cm^2, 60 s off).

the light (Figures S8). With this approach, we produced constructs with five different effectors utilizing the multi-protein chromatin modifying complex recruiters *PHO4* and *UME6*, as well as the catalytic domains known to associate with them (*ACS2*, *GCN5*, and *RPD3*) (Figure S1b-c)[45-48].

With these approaches in hand, we integrated the 5xC120 sequence near the initial Pho4 binding site in the *PHO5* promoter (green star in Figure 3a) and saw if it would alter the native expression of *PHO5* under depleted P_i conditions. Both wild type W303a and 5xC120

integrated cells were depleted of P_i and then observed for *PHO5* activation at various timepoints. mRNA levels were measured using quantitative PCR that were normalized to both ACT1 and ALG9 housekeeping genes. At 1 hour, 2 hour, and 4 hour timepoints, there was no significant difference in *PHO5* expression due to the insertion of the 5xC120 sequence. After 4 hours of gene induction, we observed an over 100-fold increase in *PHO5* transcript levels relative to control for both samples (Figure 3c).

We first deployed our catalytic domain constructs (Acs2, Gcn5, and Rpd3) under high P_i conditions (7.3 mM) targeting the *PHO5* promoter but were unsuccessful. No differences in ΔCt were observed between light and dark samples for all three constructs in relation to both the *ACT1* and *ALG9* housekeeping genes (Figure S9). These experiments were repeated in low phosphate media (50 μM P_i) targeting either the *PHO5* or *PHO84* promoters, but the results were inconclusive or unsuccessful. When comparing the ΔCt of light vs dark, there was either no differences in relative expression when compared to the housekeeping genes, or the variability was inconsistent between *ACT1* and *ALG9* (Figures S10, S11). However, when we used the new transcription factor constructs Pho4-EL222 and Ume6-EL222, opposite phenotypes were observed. As seen in the mCherry constructs, the linker used to fuse proteins to the LOV core is long enough to allow proper folding and activity. With the addition of an NLS sequence to both Pho4-EL222 and Ume6-EL222, these proteins are quickly sequestered to the nucleus of each cell. In the case of Pho4-EL222, we observed *PHO5* transcript levels at 110-fold increase relative to the NLS-EL222 controls indicating perpetual *PHO5* activation regardless of illumination (Figure 3d). These levels were nearly identical to the phosphate depleted cells after 4 hours in Figure 3c. In high P_i, Pho4 is heavily phosphorylated and kept cytosolic in yeast cells. Our data shows that both attachment to EL222 and the addition of an NLS sequence can overcome that natural repression, with enough room given by the linker for the attached Pho4 to bind to DNA on its own. By mutating a critical glutamic acid into leucine

producing Pho4^{E259L}-EL222, we successfully prevented this DNA binding in the dark. A similar issue arose with Ume6 also being active and forced nuclear when fused to EL222 but resulted in repeated lethality across all cells. After transformations in triplicate with Ume6-EL222, all plates were devoid of colonies. Ume6 is similar to the Zn2C6 GAL4 transcription factor, and so we used that protein as a guide to make a double mutation in critical cysteines responsible for DNA binding[46, 49]. Ume6$^{C770A/C787A}$-EL222 was no longer able to bind to DNA on its own, providing successful transformation colonies (Figure S12).

Activation and repression of the phosphate responsive gene *PHO5* by transcription factor, distance, and phosphate availability

First, we wanted to establish how our standard VP-EL222 was able to control gene function in a biologically simpler state. The chromatin landscape becomes much more accessible as phosphate is depleted, so we chose to lower the available P_i to a concentration of 50 μM. We used the Y421 yeast centromeric plasmid developed for expression in *S. cerevisiae,* with EL222 variants being constitutively expressed by an *A. gossypii* TEF fungal promoter (Figure S13). As a control for all *PHO5* transcript levels in Figure 4b-c, the dark state levels of VP-EL222 in high P_i at insertion point A was used. After 4 hours (20 s on at 15 mW/cm^2, 60 s off), a well-defined pattern of expression for VP-EL222 along the *PHO5* promoter emerged. VP-EL222 had a maximum effect at the A site adjacent to UASp1 with *PHO5* transcript levels increasing by 67 fold after 4 hours. As we moved farther away from the UASp1 site, VP-EL222's potency decreased, with *PHO5* transcript levels steadily dropping through sites B and C. At the farthest binding site D, the *PHO5* transcript levels remained unchanged with illumination (Figure 4b). When we raised the media [P_i] to 7.3 mM, control over gene expression dramatically changed to a level of mixed success. At the initial sites A and B, VP-EL222 induced *PHO5* approximately 8- and 4-fold after 4 hours, respectively. As the distance increased to site C, we saw a spike up to 16-fold; while we saw the largest variability in data distribution here, all points

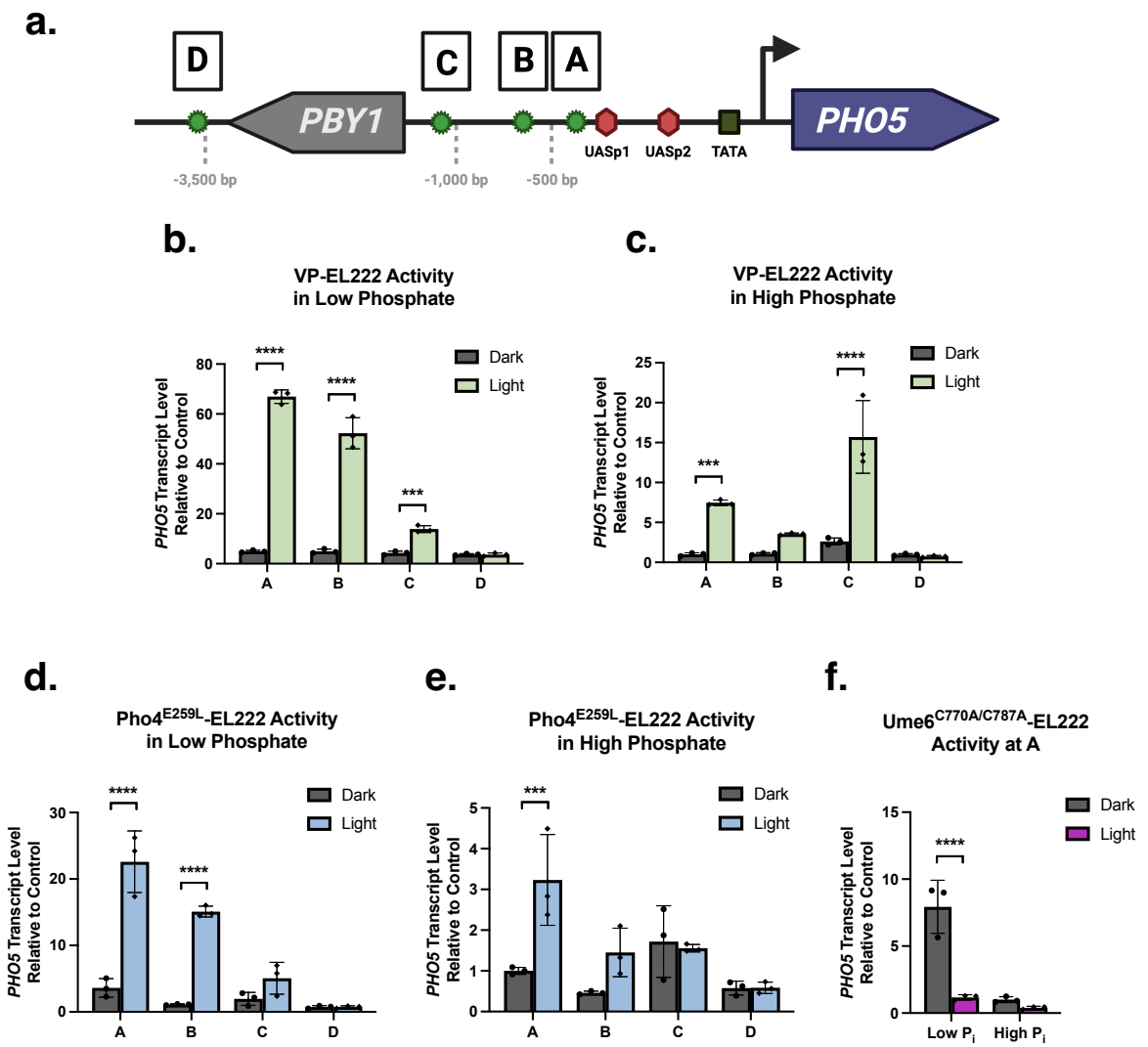

Figure 4. *PHO5* gene expression using various EL222 fusion constructs as related to both a function of distance and phosphate availability. (a) Representation of the *PHO5* promoter region with UAS sites (red hexagons) and the TATA box (black). Green stars indicate 5xC120 insertion sites along the *PHO5* promoter (A-D) with the farthest D site beyond the adjacent gene *PBY1*. (Distances from TSS: UASp1 - 361 bp , A - 414 bp, B - 560 bp, C - 1,029 bp, D - 3,510 bp). (b) VP-EL222 activity in low P_i (50 μM). (c) VP-EL222 activity in high P_i (7.3 mM). (d) Pho4^{E259L}-EL222 activity in low P_i (50 μM). (e) Pho4^{E259L}-EL222 activity in high P_i (7.3 mM). (f) Ume6$^{C770A/C787A}$-EL222 activity in low and high P_i (50 μM and 7.3 mM, respectively). Data shown are mean ± SD. Significance was calculated using Two-Way ANOVA with Turkey's multiple comparison test. *$p \leq 0.05$, **$p \leq 0.01$, ***$p \leq 0.001$, ****$p \leq 0.0001$.

were above the other samples. Site D again showed no change in *PHO5* transcript levels (Figure 4c). When comparing the dark state levels of *PHO5* activity, we observed at 4-5 fold decrease across all sites when the media [P_i] was raised from 50 μM to 7.3 mM (Figure 4b-c).

While a highly potent TAD, VP16 is not at all biologically relevant to yeast, leading us to explore how EL222-based recruitment of a native activator like Pho4 could influence the *PHO5* expression. As a reference control for all *PHO5* transcript levels in Figure 4d-e, the dark state levels of Pho4^{E259L}-EL222 in high P_i at insertion point A was used. Pho4^{E259L}-EL222 was deployed in the same fashion as VP-EL222 and produced a defined comparable pattern under lower P_i conditions. At site A, a 23 fold increase in mRNA production is observed after 4 hours. This reduced in a stepwise fashion as we moved farther away along the promoter region through sites B and C. Once again, we saw no increase in *PHO5* transcript levels for site D (Figure 4d). When the phosphate levels are raised up to 7.3 mM P_i, a similar pattern of variability emerged. Site A produced a 3 fold increase after 4 hours of blue light exposure. This dropped to negligible levels for sites B and C, with a wide distribution for dark state site C transcripts. Site D continued to show no effects here as well (Figure 4e). The broad distribution of sample points and less apparent patterns are similarly found for both VP-EL222 and Pho4^{E259L}-EL222 in high P_i. For dark state expression levels, we saw up to a 4 fold decrease across all sites when the media [P_i] was raised from 50 μM to 7.3 mM (Figure 4d-e).

To complement the above optogenetic activation approaches, we wanted to see if similar strategies would allow us to repress gene expression levels as well. To do so, we utilized the Ume6 repressor, a key transcriptional regulator of early meiotic genes in yeast[50]. This subunit is a part of the greater Rpd3S/L histone deacetylase complex and does not normally bind in the *PHO5* promoter region[51]. Utilizing a double mutant in Ume6 predicted to disrupt inherent DNA binding in this protein and fusing it to EL222, we deployed Ume6$^{C770A/C787A}$-EL222 into the A site only background cells containing the 5xC120 binding sequence. In both experiments, we used the dark state high P_i transcript levels as the control for *PHO5* mRNA expression. In low P_i, the dark state basal activity of *PHO5* expression rose by an 8 fold increase. Through binding of Ume6$^{C770A/C787A}$-EL222 at site A, we were able to repress expression of *PHO5* by nearly 8-fold back to the dark state high P_i transcript levels. But, under high P_i conditions, dark state

expression levels were significantly reduced to the point Ume6$^{C770A/C787A}$-EL222 was unable to depress them farther (Figure 4f).

Activation and repression of the phosphate responsive gene *PHO84* by transcription factor, distance, and phosphate availability

To examine the general utility of these EL222-based tools, we investigated their performance in the similarly-related gene *PHO84*. While the promoter region of PHO84 is less understood than *PHO5*, *PHO84* contains five Pho4-binding UAS sites. We inserted 5xC120 sequences into two of these sites: AA (-230 bp from the TSS) and BB (-495 bp). Site AA occupies a space between UASpE and the TATA box (where nucleosomes are known to form) that should be accessible in a repressed state, while site BB was chosen because it sits between the UASpB (occluded by a histone), and the high affinity UASpC/D which are accessible in a repressed state (Figure 5a)[2]. For both low and high P_i, we used the site AA dark state high P_i levels as the control reference for *PHO84* transcripts as it relates to each respective construct. First, VP-EL222 was used to target site AA under low P_i conditions. This produced a 9 fold increase in transcript levels when compared to the dark state. When we observed activity at site BB however, we saw no significant increase in levels. When we switched cells to high P_i (7.3 mM), we saw a 10 fold increase in transcript levels at site AA. In the light, both high and low P_i levels produced a wide distribution of datapoints with no significant difference between the two. As for site BB, there was no significant change in *PHO84* transcript production after 4 hours. When we looked at the dark state basal activity at 50 μM P_i, site BB produced over a 6 fold increase, nearly 3 times as much as the site AA dark state basal activity. At the *PHO5* promoter, nearly all the dark state basal activity was the same, regardless of position. Here, because of the earlier activity and expression gradient of *PHO84* in response

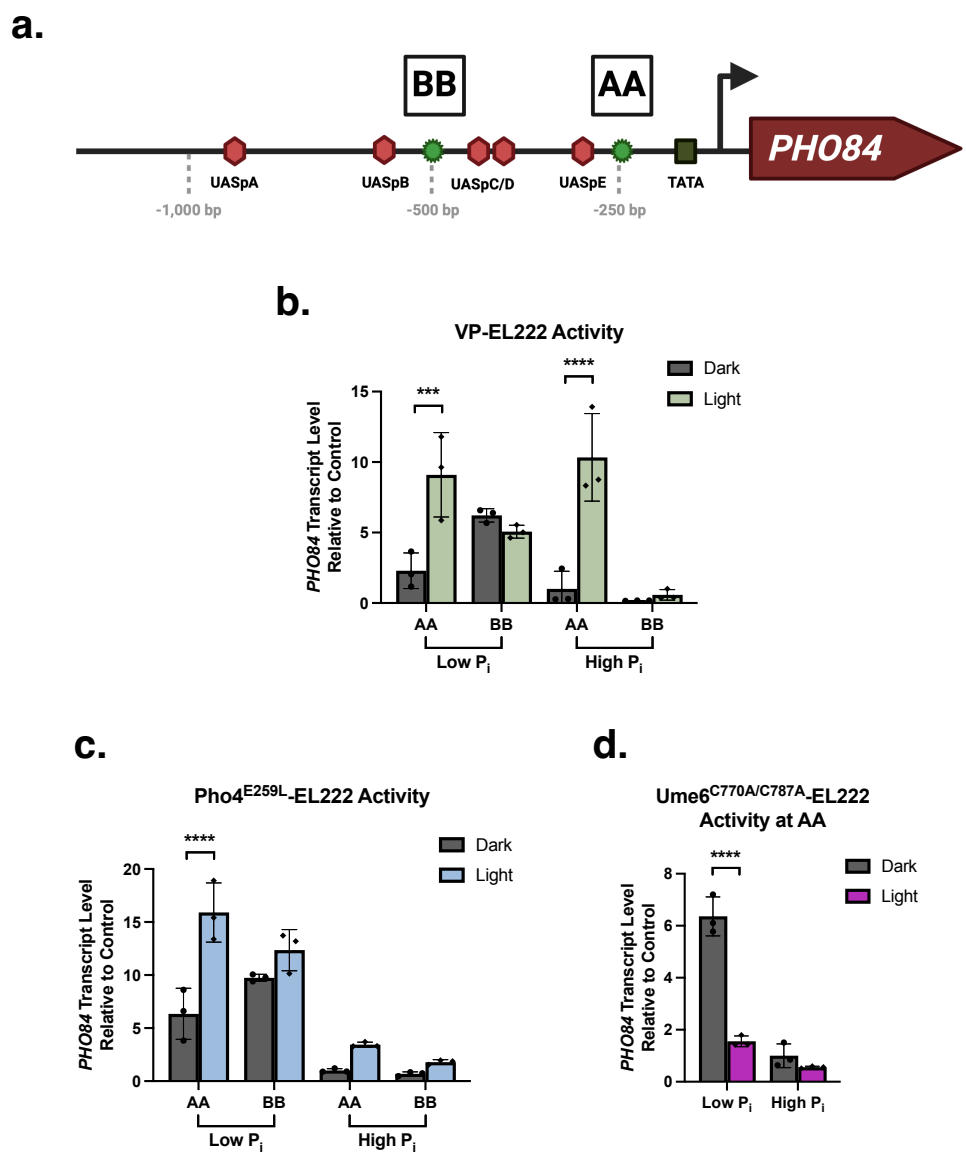

Figure 5. *PHO84* gene expression using various EL222 fusion constructs as related to both a function of distance and phosphate availability. Representation of the *PHO84* promoter region with UAS sites (red hexagons) and the TATA box (black). Green stars show 5xC120 insertion sites along the *PHO84* promoter (AA, BB). (Distances from TSS: AA - 230 bp, BB - 495 bp). (b) VP-EL222 activity in low (50 μM) and high (7.3 mM) P_i. (c) $Pho4^{E259L}$-EL222 activity in low (50 μM) and high (7.3 mM) P_i. (d) $Ume6^{C770A/C787A}$-EL222 activity in low (50 μM) and high (7.3 mM) P_i. Data shown are mean ± SD. Significance was calculated using Two-Way ANOVA with Turkey's multiple comparison test. *$p \leq 0.05$, **$p \leq 0.01$, ***$p \leq 0.001$, ****$p \leq 0.0001$.

to phosphate levels, we observed a change in this activity. But, while site AA can still significantly boost expression of *PHO84* in the light, site BB was unable to provide an increase in transcription in both cases (Figure 5b).

Next, we moved on to the native transcription factor construct Pho4^{E259L}-EL222. For site AA at low P_i levels, Pho4^{E259L}-EL222 was able to produce a 16 fold increase of mRNA production, nearly double the value of VP-EL222 in Figure 5b. However, dark state activity was also higher registering a 6-fold increase when compared to the control. Site BB once again had the highest levels of dark state activity and showed no significant difference when exposed to the light. Under high P_i conditions, both sites AA and BB were unable to produce a significant increase in *PHO84* transcript levels after 4 hours of blue light exposure when compared to the dark start reference control (Figure 5c). The strength of the VP16 TAD was able to activate transcription at site AA under high P_i conditions when Pho4^{E259L}-EL222 was unable to. Finally, we once again wanted to see if we could repress transcription of *PHO84* using Ume6$^{C770A/C787A}$-EL222. We chose to target site AA with the dark state high P_i sample acting as the reference control. When P_i was depleted to 50 μM concentrations, the dark state levels of *PHO84* increased by over 6-fold. Under 4 hours of light activation, Ume6$^{C770A/C787A}$-EL222 was able to successfully repress expression back to levels comparable to those seen in the dark state control. But, when the P_i concentrations were brought back up to 7.3 mM, gene expression was repressed and Ume6$^{C770A/C787A}$-EL222 showed no impact (Figure 5d). While the variability of the *PHO84* promoter produced results from VP-EL222 and Pho4^{E259L}-EL222 gene activation that were less apparent as the *PHO5* experiments, Ume6$^{C770A/C787A}$-EL222 was shown to repress transcription in the same fashion throughout. At both *PHO5* and *PHO84*, our repression construct was able to depress transcript levels under active conditions all the way back to levels comparable to the high P_i, repressed conditions.

DISCUSSION

We better characterized VP-EL222 on a plasmid based system using *in vivo* analyses with multiple experimental devices for illumination and readout. A proof-of-concept for N-terminally tethered EL222 fusion proteins was a success after the addition of a substantial

spacer between the extra domain and the LOV-HTH core. This led to the development of new transcriptional coactivator and corepressor EL222 fusion proteins native to the host system, *Saccharomyces cerevisiae*. We moved into genomic DNA targets through stable integration of the 5xC120 EL222 binding sequence using CRISPR, targeting the yeast phosphate stress response genes *PHO5* and *PHO84*. These chromatin driven promoter regions are accessible in a minimal phosphate environment but become increasingly more complex as phosphate becomes readily available. Initial probing with VP-EL222 was further extended by investigating these targets using non-VP effectors such as Pho4^{E259L}-EL222 and Ume6$^{C770A/C787A}$-EL222, leading to successful gene activation and repression.

We present tunable specifications for the blue-light activated transcription factor VP-EL222 in *Saccharomyces cerevisiae* using a single plasmid reporter system. A saturation point of ~1.8 mW/cm^2 was observed with a near one-to-one fold increase possible at the lowest end of the light intensity spectrum. We also confirm that pulse intensity is heavily weighted against number of photons over time as well as the off cycle length. This indicates that VP-EL222 is more resistant to change under cycling conditions and is much more tunable when focusing specifically on light intensities. A single 60 second exposure at maximum light intensity was able to produce over a 10-fold increase in YFP expression after 4 hours. This could be due to a cascading effect of active VP-EL222 at the 5xC120 promoter, the intensity of the VP domain as a TAD, and the maturation time of fluorescent proteins. Through N-terminal fusion of mCherry to the EL222 LOV-HTH core, we were able to confirm comparable activity to that of the VP-EL222 system and visualize proper functionality of the tethered protein. At 1,029 residues (111.2 kDa), the VP-Acs2-EL222 construct is one of the largest fusions of EL222 to be shown efficiently driving transcription. Tethering multiple domains together through a string of $(GGGGS)_9$ linkers, however, was unsuccessful (Figure S6). These constructs mostly likely have become too complex for proper protein folding and activity.

These experiments became a proof-of-concept for EL222's ability to translocate fused cargo to a specified region in the genome. We developed a plug-and-go plasmid system named "Y423" where effectors could be switched in and out with relative ease using standard molecular cloning techniques. Through CRISPR gene editing, the EL222 binding sequence 5xC120 was successfully integrated into various locations along the *PHO5* and *PHO84* promoters. Based on our initial assessments, these insertions had no effect on the native gene activation. We report here that the forced nuclear localization of Pho4 while fused to EL222 was enough to overcome the repressive phosphorylation under high phosphate conditions. This protein became active in the dark producing equal levels of *PHO5* transcripts as the wild type after 4 hours of depleted [P_i] media. Interestingly, we were able to confirm previous observations of Ume6's overexpression lethality through failed transformations[52]. Upon mutation of key cysteine residues involved in DNA binding, these cells became viable and were able to grow effectively.

The regulation and expression of *PHO* genes involved in the management of inorganic phosphate within the cell have always been stochastic in nature involving intrinsic noise[1]. We investigated their regulation optogenetically through multiple effector domains in fusions constructs with EL222 focusing on chromatin modifying complex recruiters and the catalytic domains known to associate with them. Unfortunately, our catalytic domain constructs consisting of Acs2, Gcn5, and Rpd3 were unable to alter gene activity at either promoter. We had hoped our sub-cellular localization of Acs2 to the chromatin would act in a similar manner to its mammalian homolog ACSS2[53] and assist in Acetyl-CoA production for histone acetylation but were unsuccessful. Some enzymes like Gcn5 are weak on their own and require the formation of subcomplexes for robust acetylation of nucleosomes[31, 54]. For our gene targets, these catalytic domains alone were insufficient to control gene function and mostly likely were unable to recruit other necessary components themselves. Multi-domain complexes are involved in chromatin remodeling, which is why when we deployed our transactivation domain constructs, we were successful in altering gene activity. We were able to show that under low P_i conditions,

a clear and defined pattern of *PHO5* control emerged for both VP-EL222 and Pho4^{E259L}-EL222. Sites closest to the UASp1 induced the highest levels of *PHO5* transcripts, with a descending gradient pattern forming as the 5xC120 sites were moved farther away. As the available phosphate was increased to 7.3 mM, the conditions become much more repressive. The complexity of the chromatin arrangement leads to variability in both accessibility and effectiveness at activating the system. Light induced VP-EL222 and Pho4^{E259L}-EL222 formed little discernable patterns when activated across the promoter region, with a severely reduced capacity for transcription activation overall. In one case, VP-EL222 had the highest activation -1,029 bp away from the TSS while Pho4^{E259L}-EL222 was most effective adjacent the UASp1 site at -414 bp from the TSS. At a max distance of -3,510 bp located a full gene away, no effect can be seen on gene activity. We did observe a 4-5 fold increase of low P_i *PHO5* dark state activity across all sites when compared to the high P_i levels. This is probably due to some of the native nuclear Pho4 proteins becoming completely dephosphorylated and inducing low levels of activity[40, 42]. Hence, the chromatin state of the *PHO5* promoter is more accessible under low phosphate conditions and is why we see such a dramatic increase in coactivator driven transcript levels at sites A and B[27]. It is also worth noting, we do not know if the Pho4^{E259L} bound protein interacts with the nuclear Pho4 in low phosphate conditions. It is possible a knock-out of native Pho4 could reduce the *PHO5* expression seen here if this is the case.

The largest variability between VP-EL222 and Pho4^{E259L}-EL222 was observed at the *PHO84* promoter, revealing the nuance between native and non-native effectors. Interestingly, VP-EL222 in the light produced the same levels of expression at site AA for both high and low P_i. This is an alternative trend to the one observed up to this point for both VP-EL222 and Pho4^{E259L}-EL222 at the *PHO5* promoter. Knowing that *PHO84* is more active at 50 μM P_i, this indicates that VP-EL222's activity at site AA is unaffected by chromatin structure. Conversely, Pho4^{E259L}-EL222 followed the same trend in relation to phosphate availability as was seen in *PHO5*. As for the complete lack of site BB light-state activity, we still observe higher levels of

dark state expression indicating the 5xC120 stable integration is most likely not the issue. Regardless of N-terminal effector used, this site is either unbound, negatively interacting with other DNA bound factors, or just is unable to drive transcription at this exact position regardless of P_i induced promoter arrangement. Pho4^{E259L}-EL222 offers a native approach to gene activation and could be influenced by the other cofactors that interact with Pho4 protein within the cell. This is important when trying to understand complex chromatin systems like the *PHO* regulon with minimal invasiveness. While VP-EL222 was a stronger activator overall, this does not always make it the optimal choice as it lacks biological relevance to yeast. There have also been reports of VP16's toxicity in certain organisms, requiring alternative options and highlighting the importance when choosing a transcription factor[12].

Not only were we able to control gene activation using multiple coactivator fusion proteins, but we were also able to repress gene activity using the corepressor fusion construct Ume6$^{C770A/C787A}$-EL222. While Pho4 is the traditional binding partner to the *PHO5* and *PHO84* promoters, Ume6 does not traditionally bind here. Ume6$^{C770A/C787A}$-EL222 was able to repress gene activity under low P_i conditions back to the control levels seen in the high P_i dark levels. This up to 8-fold decrease indicates not only a return to an off state, but the potential at other promoters to repress at an even greater fold intensity. We attribute this to most likely occurring by Ume6$^{C770A/C787A}$-EL222 recruiting the full histone deacetylase complex and actively repressing transcription through chromatin remodeling back to the off state. However, we cannot presently rule out this occurring instead through a passive mechanism, e.g. steric occlusion by the recruitment of certain Ume6-associated factors that simply block access to the transcription site.

In conclusion, we not only define a new set of parameters for novel engineered EL222 optogenetic tools, but also apply them strategically to investigate dynamic gene promoters. We present our plasmid based systems which can be manipulated using blue-light illumination in multiple experimental set-ups. With the stable insertion into any genome of the 5xC120 binding sequence, different effector-EL222 constructs can be transiently expressed with ease to target

the same site under different environmental conditions. Here, we show the yeast *PHO5* and *PHO84* promoters are less definable using light induced gene activation under high P_i, repressed conditions. This seems congruent with the stochastic nature of the chromatin landscape that controls the mechanisms of activity. These genes can be controlled by phosphate levels as well as distance, acting in a gradient, with activity based on strength of transcriptional activating effectors or repressors. *PHO84*'s gradient like response to phosphate levels and the complex nature of its promoter shows how multivariate gene expression can be, even in tightly control optogenetic experiments. Not only was our probing of the *PHO* genes a success, but this also continues to present a proof-of-concept for an EL222 plug-and-go system for a wide range of N-terminally fused effector domains.

MATERIALS AND METHODS

Yeast strains, media, and transformations

All *in vivo* experiments were performed using the budding yeast *Saccharomyces cerevisiae* ATCC 208352 strain W303-1a (gifted to us from Dr. Peter Lipke at Brooklyn College). Media used in this study was either YPD (1% yeast extract, 2% peptone, 2% glucose) supplemented with adenine (4 g/L), tryptophan (8 g/L), and uracil (2 g/L) or standard synthetic media (complete, tryptophan, or uracil deficient). For the phosphate mediated experiments, yeast nitrogen base without amino acids and phosphate (Formedium CYN08**) was used to create standard synthetic media (complete or tryptophan deficient) which could then be supplemented with the experimental concentrations of phosphate (0 μM, 50 μM, and 7.3 mM).

For transformations, *S. cerevisiae* W303a cells were plated on YPD agar (2% agar) and grown at 30 °C. 30 mL cultures of YPD broth were inoculated using a single colony from each plate and grown overnight at 200 rpm/30 °C. Cultures were diluted in the morning to an OD_{600} of 0.2 in 50m mL YPD broth and left to grow at 200 rpm/30 °C until an OD_{600} of 0.4-0.5 was reached (~2-3 hours). Cells were then harvested by centrifugation (4,000 rpm/ 5 min), washed

with 20 mL of ice-cold sterilized ddH_2O, and centrifuged again (4,000 rpm/ 5 min). Cell pellets were resuspended in a 20 mL solution of 0.1 M Lithium Acetate, 0.8 M Sorbitol, and 1xTE buffer for 30 min at 30 °C followed by the addition of 0.2 mL of 1 M DTT for 15 min at 30 °C. Cells were centrifuged (4,000 rpm/5 min), washed twice with 20 mL of ice-cold 1M sorbitol, and then resuspended in 0.2 mL ice-cold 1 M sorbitol.

For each yeast transformation by electroporation, 45 µL of cell suspension was combined with 5 µL of plasmid (400 ng/µL;~10kb) in a microfuge tube and left to incubate on ice for 15 min For CRISPR gene editing, 4 µL of plasmid (400 ng/µL;~10kb) and 6 µL of DHR cassette was used with 40 µL of cell suspension was used instead. Cell suspensions were transferred to 0.2 cm electroporation cuvettes and electroporated using a BioRad Gene Pulser xCell on its pre-set *S. cerevisiae* protocol (1.5 kV, 200 mA, 25 µF). Post electroporation, the cells were immediately resuspended in 1 mL of 1 M sorbitol and left to recover at 30 °C for 1 hour. Cells were centrifuged (4,000 rpm/5 min), resuspended in 200 µL 1 M sorbitol, and spread on tryptophan or uracil deficient synthetic drop out agar for selection based on the plasmid used.

Plasmids, assembly of fusion constructs, and CRISPR genome editing

Yeast centromere plasmids Y421 and Y422 (provided by Farren Isaacs, Yale University) were utilized with tryptophan auxotrophic markers (Figures S13 and 1b, respectively). Y421 and Y422 both contain a constitutively active TEF fungal promoter that drives EL222 production, but Y422 contains an additional 5 tandem repeat of EL222's (UniProt ID: Q2NB98) DNA binding sequence C120 (5XC120) upstream of the Yellow Fluorescent Protein (YFP) sequence[10]. Y422 was used to make all the fusion constructs through primer design and PCR mediated sequencing editing. Additions to the plasmid were made through targeted PCR of the backbone plasmid and desired insert followed by restriction enzyme digestion and ligation using Quick Ligase (NEB Catalog #M2200). Plasmid backbones were extracted using a Monarch Gel

Extraction kit (NEB Catalog #T1020). Effector domain sequences (ACS2, GCN5, RPD3, PHO4, and UME6) were taken straight from the host yeast cells genomic DNA by PCR for ligation in Y422. Targeted residue mutations within effector domains (Figure S1b-c) were produced via site-directed mutagenesis[55, 56] followed by DpnI digest and ligation with Quick Ligase (NEB Catalog #M2200). Alternately, a standard mCherry sequence was used in the double fluorescence constructs (Table S1; Supplemental Sequence S1).

All linkers, scaffolds, and CRIPSR HDR cassettes were produced either through gene fragment synthesis ordered from Twist Biosciences, or through PCR, RE digest, and ligation into the plasmid pHisGB1. Desired sequences where then amplified from these templates using PCR. Subtractions from these plasmids was performed using PCR primers designed with restriction enzyme sites for partial plasmid sequence amplification followed by restriction enzyme digest (including DpnI) and ligation. Final constructs were produced through the removal of Y422's 5xC120-YFP sequences creating a set of plasmids named Y423 (Figure 3b). Y421 had its VP16 sequence removed to create the NLS-EL222 "Empty" construct.

For CRISPR gene editing, the "plug-and-go" plasmid pML104 was ordered from Addgene (a gift from John Wyrick [Washington State University] Addgene plasmid #67638; http://n2t.net/addgene:67638; RRID:Addgene_67638) containing the Cas9 protein, guide RNA expression cassette with BclI-SwaI cloning sites for guide sequence cloning, and a URA3 uracil marker for yeast transformation[57]. The 20 bp guide RNA sequences were designed using CHOPCHOP[58-60], placed in oligonucleotide sequences, and ordered from IDT. Oligonucleotides were annealed in a thermocycler to themselves and used as inserts into the pML104 plasmid using Quick Ligase (Table S1). For stable integration of the 5XC120 EL222 binding sequence into the *PHO5* and *PHO84* promoter regions, DHR cassettes were designed with the desired sequence sandwiched between homology arms (~150 - 300 bp each) identical to the genomic DNA flanking the insertion point (Table S1). pML104 and the corresponding DHR cassette were co-transformed into yeast cells where the insert was integrated into the genome via double

homologous recombination (Figure S7). All plasmid described here were proliferated in *Escherichia coli* DH5α cells and subsequently purified with a Promega Wizard Genomic DNA Purification Kit (Catalog #A1120). All plasmid alterations, ordered inserts, and CRISPR genomic editing was confirmed through Sanger sequencing (GENEWIZ).

Genomic DNA and RNA extractions

For genomic DNA extractions, yeast cells were grown overnight (200 rpm/30 °C) to a required density of OD_{600} 1.0-2.0. Cells were pelleted in a 2 mL Eppendorf tube, the supernatant discarded, and the cell pelleted resuspended in 1.0 mL of DNA extraction buffer (50 mm Tris HCl, 10 mM EDTA, 50 mM NaCl, 1% [w/v] SDS, pH 7.5). "250 µL" (by volume) of sterile glass beads 425-600 µm (Sigma G8772) was added and vortex for 30 seconds to break up the yeast cells followed by incubation at 65 °C for 30 minutes. Samples were centrifuged (13,000 rpm/10 min) and 600 µL of supernatant was removed and placed in a new tube. 600 µL of phenol:chloroform:isoamyl alcohol (25:24:1 v/v/v) was added, inverted several times to mix, and centrifuged (13,000 rpm/10 min). The upper aqueous phase was removed, mixed with 0.7 volumes of cold isopropanol in a new tube, and incubated at - 20 °C for 1 hour. Samples were centrifuged (13,000 rpm/10 min), supernatant discarded, cell pellet washed with 700 µL of 70% ethanol and centrifuged again (13,000 rpm/10 min). The 70% ethanol was removed, and the cell pellet was allowed to dry in the fume hood before being resuspended in sterilized ddH_2O.

For RNA extractions, cells were flash frozen until every sample was ready for extraction. Cells were thawed on ice and the RNA was extracted using a RiboPure Yeast RNA purification kit (Invitrogen; Catalog #AM1926) as per the manufacturer's instructions. RNA samples were then flash frozen in liquid N_2 for later use in cDNA production and qPCR analysis.

Blue light illumination of samples

All *S. cerevisiae* strains were grown in 20 mL liquid cultures inoculated with single colonies and grown overnight in total darkness (200 rpm/30 °C). Cultures were diluted in the morning to an OD_{600} of 0.2 and left to grow at 200 rpm/30 °C until an OD_{600} of 0.3-0.4 was reached (~2 hours). Cell cultures were then distributed in an identical pattern into either two Corning Black with Clear Flat Bottom 96-well plates at 100 µL per well or Clear 24-well plates at 800 µL per well. One plate was covered with aluminum foil and set aside as a dark control. For the 96-well plates only, each experiment was placed on a custom built 96-well LED system (courtesy of M. Bikson, CCNY Department of Biomedical Engineering) in the dark and covered with a red-coated piece of board. 96 individual WS2812B LEDs fed into fiberoptic wires deliver independently controllable light conditions controlled by an Arduino UNO microcontroller. Blue light is emitted from these LEDs at a peak wavelength of 464.7 nm (read by an OceanOptics spectrophotometer) with a light intensity of 0.04-9.22 mW/cm^2 (Figure S3). The light plate was exposed to repeating cycles of blue light (20 s on/60 s off) for up to 4 hours. For the phosphate based experiments, a blue LED panel (465 nm, 13.8 Watts; 2501BU - LED Wholesalers) was suspended ~6 inches from the top of the 24-well plates with a light intensity of 15 mW/cm^2 and set to repeating cycles of blue light (20 s on/60 s off) using an electronic intervalometer (Model 451, GraLab) (Figure S14).

Fluorescence analysis by plate reader, flow cytometry, and microscopy

For whole well reads, a SpectraMax i3 multimode microplate reader (Molecular Devices) was used to analyze fluorescence intensity. Cells were first resuspended using a multi-channel pipette before loading into the plate reader and the data was analyzed using GraphPad Prism software. For flow cytometry, samples were analyzed using a BD Accuri C6 Sampler Plus flow cytometer, light plate first, followed by unwrapping of the dark plate. All wells were resuspended using a multi-channel pipette at a maximum of 6 wells per read to prevent variations in cell sedimentation. 20,000 events were collected per well at a threshold of 50,000 under slow flow.

Standard gating techniques were used to select single-cell yeast populations and applied to subsequent FITC channel (533/30 filter) histograms used to detect the presence of YFP (Figure S2). Data was then processed using FlowJo software[61]. mCherry fluorescence was observed using either a wide-field Axio Observer.Z1/7 Inverted Microscope (Zeiss) with a Plan-Apochromat 63x/1.40 numerical aperture (NA) oil objective or a Marianas Spinning Disk confocal microscope (Intelligent Imagine Innovations) consisting of a spinning disk confocal head (CSU-X1, Yokagawa) on a Zeiss Axio Observer inverted microscope equipped with x100/1.46 numerical aperture (NA) Plan-Apochromat (oil immersion). Frames were captured on an Axiocam 506 mono (Zeiss) using Zen software (Zeiss) for the wide-field and a Prime sCMOS camera (Photometrics) controlled by SlideBook 6 (Intelligent Imagine Innovations) for the spinning disk confocal and further processed using ImageJ[62, 63]. DAPI staining was performed using a final concentration of 10 µg/mL added to mid log-phase cells (OD_{600} of ~0.5) and let sit for 10 minutes. Cells were then harvested by centrifugation (4,000 rpm/5 min), washed with 1xPBS, centrifuged again (4,000 rpm/5 min), and resuspended in 1xPBS before imaging.

EL222 fusion protein experiments at the *PHO5* and *PHO84* promoters with quantitative PCR

All 5xC120-*PHO5* and 5xC120-*PHO84* integrated *S. cerevisiae* strains containing their respective fusion constructs were grown in 20 mL liquid cultures inoculated with single colonies and grown overnight in total darkness (200 rpm/30 °C). Cultures were diluted in the morning to an OD_{600} of 0.2 and left to grow at 200 rpm/30 °C until an OD_{600} of 0.3-0.4 was reached (~2 hours). Cell cultures were then distributed in an identical pattern into two Corning Black with Clear Flat Bottom 96-well plates at 100 µL per well or Clear 24-well plates at 800 µL per well. One plate was covered with aluminum foil and set aside as a dark control. The other plate was illuminated as outlined previously. Samples were collected and flash frozen in liquid N_2 for later

use. Samples were then thawed, and the RNA was extracted from each sample as outlined previously.

RNA for each sample was diluted to a total concentration of 500 ng in 16 µL with 4 µL of qScript Ultra SuperMix (Quantabio #95217) added for a total of 20 µL. Samples were run in a thermocycler for a single cycle (2 min/25 °C, 10 min/55 °C, 1 min/95 °C) to create 500 ng of cDNA. These samples were diluted down to a concentration of 1 ng/µL and distributed into a 384-well plate in triplicate (5 µL per well). Genes are targeted using primer pairs to produce sequence lengths of ~100-300 bp (*PHO5* or *PHO84* and two housekeeping gene controls *ACT1* and *ALG9*) (Table S1)[64-66]. Both forward and reverse primers were mixed in the same tube to a stock concertation of 10 µM. 7 µL of master mix (6 µL PerfeCTa SYBR Green FastMix [Quantabio #95071], 0.5 µL primer stock, 0.5 µL dd H_2O) was added to each sample well for a total volume of 12 µL per well. The plate was then sealed and analyzed using a QuantStudio 7 Flex Real-time qPCR system. For experiments performed in biological triplicates, data was analyzed using the $2^{-\Delta\Delta CT}$ method with the geometric mean of both *ACT1* and *ALG9* housekeeping gene controls. For the technical replicates of n = 1, data was analyzed using the ΔCT of each housekeeping gene control.

ASSOCIATED CONTENT

Supporting Information

Supplemental Figures S1-S14, Table S1, and Sequence S1 are provided as a compilation of in-depth resources to assist in any technical questions based on the main publication. This includes outlines of all the constructs used in this study along with a reference sequence, supporting flow cytometry/qPCR data, and technical specifications for major points provided in the text.

AUTHOR INFORMATION

Matthew M. Cleere - Structural Biology Initiative, CUNY Advanced Science Research Center, New York, NY 10031; Biology Ph.D. Program, Graduate Center, City University of New York, New York, NY 10016; https://orcid.org/0000-0003-3285-6949

Kevin H. Gardner - *Structural Biology Initiative, CUNY Advanced Science Research Center, New York, NY 10031; Biochemistry, Chemistry, and Biology Ph.D. Programs, Graduate Center, City University of New York, New York, NY 10016; Department of Chemistry and Biochemistry, City College of New York, New York, NY 10031*; https://orcid.org/0000-0002-8671-2556; Email: kgardner@gc.cuny.edu

Author Contributions

M.M.C.: conceptualization, investigation, formal analysis, writing; K.H.G.: conceptualization, supervision, editing, funding.

Funding

This work was funded by the National Institutes of Health grant R01 GM106239.

Notes

The authors declare no competing financial interest.

ACKNOWLEDGEMENTS

We thank Farren Isaacs (Yale University, Yale School of Medicine) for gifting the Y421 and Y422 plasmids and Peter Lipke (Brooklyn College, School of Natural and Behavioral Sciences) for supplying the W303a *S. cerevisiae* strains used in this study. We thank Marom Bikson and Robin Azzam (CCNY, Department of Biomedical Engineering) for the custom 96-well LED

machine. We thank Alfredo Vidal Ceballos and Rachel Fisher (CUNY Advanced Science Research Center) for assistance with the wide-field and confocal microscopy. We would also like to thank Jia Liu, Catherine Leckie, and Sami Sauma for their assistance with quantitative PCR. Graphical abstract and Figures 3a, 4a, 5a, and S7 were all created with BioRender.com. Plasmid maps found in Figures 1b, 3b, and S13 were all created with AngularPlasmid.

REFERENCES

[1] Korber, P., and Barbaric, S. (2014) The yeast PHO5 promoter: from single locus to systems biology of a paradigm for gene regulation through chromatin, *Nucleic Acids Res 42*, 10888-10902.

[2] Wippo, C. J., Krstulovic, B. S., Ertel, F., Musladin, S., Blaschke, D., Sturzl, S., Yuan, G. C., Horz, W., Korber, P., and Barbaric, S. (2009) Differential cofactor requirements for histone eviction from two nucleosomes at the yeast PHO84 promoter are determined by intrinsic nucleosome stability, *Mol Cell Biol 29*, 2960-2981.

[3] Fascher, K. D., Schmitz, J., and Horz, W. (1993) Structural and Functional Requirements for the Chromatin Transition at the Pho5 Promoter in Saccharomyces-Cerevisiae Upon Pho5 Activation, *J Mol Biol 231*, 658-667.

[4] Losi, A., Gardner, K. H., and Moglich, A. (2018) Blue-Light Receptors for Optogenetics, *Chem Rev 118*, 10659-10709.

[5] Nash, A. I., McNulty, R., Shillito, M. E., Swartz, T. E., Bogomolni, R. A., Luecke, H., and Gardner, K. H. (2011) Structural basis of photosensitivity in a bacterial light-oxygen-voltage/helix-turn-helix (LOV-HTH) DNA-binding protein, *Proc Natl Acad Sci U S A 108*, 9449-9454.

[6] Swartz, T. E., Tseng, T. S., Frederickson, M. A., Paris, G., Comerci, D. J., Rajashekara, G., Kim, J. G., Mudgett, M. B., Splitter, G. A., Ugalde, R. A., Goldbaum, F. A., Briggs, W. R., and Bogomolni, R. A. (2007) Blue-light-activated histidine kinases: two-component sensors in bacteria, *Science 317*, 1090-1093.

[7] Taylor, B. L., and Zhulin, I. B. (1999) PAS domains: internal sensors of oxygen, redox potential, and light, *Microbiol Mol Biol Rev 63*, 479-506.

[8] Zoltowski, B. D., Schwerdtfeger, C., Widom, J., Loros, J. J., Bilwes, A. M., Dunlap, J. C., and Crane, B. R. (2007) Conformational switching in the fungal light sensor vivid, *Science 316*, 1054-1057.

[9] Zoltowski, B. D., Nash, A. I., and Gardner, K. H. (2011) Variations in protein-flavin hydrogen bonding in a light, oxygen, voltage domain produce non-Arrhenius kinetics of adduct decay, *Biochemistry 50*, 8771-8779.

[10] Motta-Mena, L. B., Reade, A., Mallory, M. J., Glantz, S., Weiner, O. D., Lynch, K. W., and Gardner, K. H. (2014) An optogenetic gene expression system with rapid activation and deactivation kinetics, *Nat Chem Biol 10*, 196-202.

[11] Reade, A., Motta-Mena, L. B., Gardner, K. H., Stainier, D. Y., Weiner, O. D., and Woo, S. (2017) TAEL: a zebrafish-optimized optogenetic gene expression system with fine spatial and temporal control, *Development 144*, 345-355.

[12] LaBelle, J., Ramos-Martinez, A., Shen, K., Motta-Mena, L. B., Gardner, K. H., Materna, S. C., and Woo, S. (2021) TAEL 2.0: An Improved Optogenetic Expression System for Zebrafish, *Zebrafish 18*, 20-28.

[13] Zhao, E. M., Lalwani, M. A., Chen, J. M., Orillac, P., Toettcher, J. E., and Avalos, J. L. (2021) Optogenetic Amplification Circuits for Light-Induced Metabolic Control, *ACS Synth Biol 10*, 1143-1154.

[14] Rullan, M., Benzinger, D., Schmidt, G. W., Milias-Argeitis, A., and Khammash, M. (2018) An Optogenetic Platform for Real-Time, Single-Cell Interrogation of Stochastic Transcriptional Regulation, *Mol Cell 70*, 745-756 e746.

[15] Jayaraman, P., Devarajan, K., Chua, T. K., Zhang, H., Gunawan, E., and Poh, C. L. (2016) Blue light-mediated transcriptional activation and repression of gene expression in bacteria, *Nucleic Acids Res 44*, 6994-7005.
[16] Rivera-Cancel, G., Motta-Mena, L. B., and Gardner, K. H. (2012) Identification of natural and artificial DNA substrates for light-activated LOV-HTH transcription factor EL222, *Biochemistry 51*, 10024-10034.
[17] Zhao, E. M., Zhang, Y., Mehl, J., Park, H., Lalwani, M. A., Toettcher, J. E., and Avalos, J. L. (2018) Optogenetic regulation of engineered cellular metabolism for microbial chemical production, *Nature 555*, 683-687.
[18] Baaske, J., Gonschorek, P., Engesser, R., Dominguez-Monedero, A., Raute, K., Fischbach, P., Muller, K., Cachat, E., Schamel, W. W. A., Minguet, S., Davies, J. A., Timmer, J., Weber, W., and Zurbriggen, M. D. (2018) Dual-controlled optogenetic system for the rapid down-regulation of protein levels in mammalian cells, *Sci Rep-Uk 8*.
[19] Benzinger, D., and Khammash, M. (2018) Pulsatile inputs achieve tunable attenuation of gene expression variability and graded multi-gene regulation, *Nat Commun 9*, 3521.
[20] Guerra, P., Vuillemenot, L. A., Rae, B., Ladyhina, V., and Milias-Argeitis, A. (2022) Systematic In Vivo Characterization of Fluorescent Protein Maturation in Budding Yeast, *ACS Synth Biol 11*, 1129-1141.
[21] Gligorovski, V., Sadeghi, A., and Rahi, S. J. (2023) Multidimensional characterization of inducible promoters and a highly light-sensitive LOV-transcription factor, *Nat Commun 14*, 3810.
[22] Rando, O. J., and Winston, F. (2012) Chromatin and transcription in yeast, *Genetics 190*, 351-387.
[23] Yadav, K. K., Singh, N., and Rajasekharan, R. (2016) Responses to phosphate deprivation in yeast cells, *Curr Genet 62*, 301-307.
[24] Barbaric, S., Reinke, H., and Hörz, W. (2003) Multiple mechanistically distinct functions of SAGA at the promoter, *Mol Cell Biol 23*, 3468-3476.
[25] Reinke, H., and Horz, W. (2003) Histones are first hyperacetylated and then lose contact with the activated PHO5 promoter, *Mol Cell 11*, 1599-1607.
[26] Komeili, A., and O'Shea, E. K. (1999) Roles of phosphorylation sites in regulating activity of the transcription factor Pho4, *Science 284*, 977-980.
[27] Boeger, H., Griesenbeck, J., Strattan, J. S., and Kornberg, R. D. (2003) Nucleosomes unfold completely at a transcriptionally active promoter, *Mol Cell 11*, 1587-1598.
[28] Boeger, H., Griesenbeck, J., Strattan, J. S., and Kornberg, R. D. (2004) Removal of promoter nucleosomes by disassembly rather than sliding in vivo, *Mol Cell 14*, 667-673.
[29] Cheon, Y., Kim, H., Park, K., Kim, M., and Lee, D. (2020) Dynamic modules of the coactivator SAGA in eukaryotic transcription, *Exp Mol Med 52*, 991-1003.
[30] Espinola-Lopez, J. M., and Tan, S. (2021) The Ada2/Ada3/Gcn5/Sgf29 histone acetyltransferase module, *Bba-Gene Regul Mech 1864*.
[31] Sun, J., Paduch, M., Kim, S. A., Kramer, R. M., Barrios, A. F., Lu, V., Luke, J., Usatyuk, S., Kossiakoff, A. A., and Tan, S. (2018) Structural basis for activation of

SAGA histone acetyltransferase Gcn5 by partner subunit Ada2, *Proc Natl Acad Sci U S A 115*, 10010-10015.
[32] van den Berg, M. A., de Jong-Gubbels, P., Kortland, C. J., van Dijken, J. P., Pronk, J. T., and Steensma, H. Y. (1996) The two acetyl-coenzyme A synthetases of Saccharomyces cerevisiae differ with respect to kinetic properties and transcriptional regulation, *J Biol Chem 271*, 28953-28959.
[33] Takahashi, H., McCaffery, J. M., Irizarry, R. A., and Boeke, J. D. (2006) Nucleocytosolic acetyl-coenzyme A synthetase is required for histone acetylation and global transcription, *Mol Cell 23*, 207-217.
[34] Mutlu, B., and Puigserver, P. (2021) GCN5 acetyltransferase in cellular energetic and metabolic processes, *Biochim Biophys Acta Gene Regul Mech 1864*, 194626.
[35] Kadosh, D., and Struhl, K. (1997) Repression by Ume6 involves recruitment of a complex containing Sin3 corepressor and Rpd3 histone deacetylase to target promoters, *Cell 89*, 365-371.
[36] Yeheskely-Hayon, D., Kotler, A., Stark, M., Hashimshony, T., Sagee, S., and Kassir, Y. (2013) The roles of the catalytic and noncatalytic activities of Rpd3L and Rpd3S in the regulation of gene transcription in yeast, *PLoS One 8*, e85088.
[37] Ohlendorf, R., and Moglich, A. (2022) Light-regulated gene expression in Bacteria: Fundamentals, advances, and perspectives, *Front Bioeng Biotechnol 10*, 1029403.
[38] Lo, C. L., Choudhury, S. R., Irudayaraj, J., and Zhou, F. C. (2017) Epigenetic Editing of Ascl1 Gene in Neural Stem Cells by Optogenetics, *Sci Rep 7*, 42047.
[39] Oshima, Y. (1997) The phosphatase system in Saccharomyces cerevisiae, *Genes Genet Syst 72*, 323-334.
[40] Springer, M., Wykoff, D. D., Miller, N., and O'Shea, E. K. (2003) Partially phosphorylated Pho4 activates transcription of a subset of phosphate-responsive genes, *PLoS Biol 1*, E28.
[41] Han, M., and Grunstein, M. (1988) Nucleosome loss activates yeast downstream promoters in vivo, *Cell 55*, 1137-1145.
[42] Thomas, M. R., and O'Shea, E. K. (2005) An intracellular phosphate buffer filters transient fluctuations in extracellular phosphate levels, *Proc Natl Acad Sci U S A 102*, 9565-9570.
[43] Adkins, M. W., Williams, S. K., Linger, J., and Tyler, J. K. (2007) Chromatin disassembly from the PHO5 promoter is essential for the recruitment of the general transcription machinery and coactivators, *Mol Cell Biol 27*, 6372-6382.
[44] Ogawa, N., Saitoh, H., Miura, K., Magbanua, J. P., Bun-ya, M., Harashima, S., and Oshima, Y. (1995) Structure and distribution of specific cis-elements for transcriptional regulation of PHO84 in Saccharomyces cerevisiae, *Mol Gen Genet 249*, 406-416.
[45] Fisher, F., and Goding, C. R. (1992) Single amino acid substitutions alter helix-loop-helix protein specificity for bases flanking the core CANNTG motif, *EMBO J 11*, 4103-4109.
[46] Gardner, K. H., Pan, T., Narula, S., Rivera, E., and Coleman, J. E. (1991) Structure of the binuclear metal-binding site in the GAL4 transcription factor, *Biochemistry 30*, 11292-11302.

[47] Li, X., Yu, W., Qian, X., Xia, Y., Zheng, Y., Lee, J. H., Li, W., Lyu, J., Rao, G., Zhang, X., Qian, C. N., Rozen, S. G., Jiang, T., and Lu, Z. (2017) Nucleus-Translocated ACSS2 Promotes Gene Transcription for Lysosomal Biogenesis and Autophagy, *Mol Cell 66*, 684-697 e689.

[48] Wang, L., Liu, L., and Berger, S. L. (1998) Critical residues for histone acetylation by Gcn5, functioning in Ada and SAGA complexes, are also required for transcriptional function in vivo, *Genes Dev 12*, 640-653.

[49] Anderson, S. F., Steber, C. M., Esposito, R. E., and Coleman, J. E. (1995) UME6, a negative regulator of meiosis in Saccharomyces cerevisiae, contains a C-terminal Zn2Cys6 binuclear cluster that binds the URS1 DNA sequence in a zinc-dependent manner, *Protein Sci 4*, 1832-1843.

[50] Strich, R., Surosky, R. T., Steber, C., Dubois, E., Messenguy, F., and Esposito, R. E. (1994) UME6 is a key regulator of nitrogen repression and meiotic development, *Genes Dev 8*, 796-810.

[51] Rundlett, S. E., Carmen, A. A., Suka, N., Turner, B. M., and Grunstein, M. (1998) Transcriptional repression by UME6 involves deacetylation of lysine 5 of histone H4 by RPD3, *Nature 392*, 831-835.

[52] Washburn, B. K., and Esposito, R. E. (2001) Identification of the Sin3-binding site in Ume6 defines a two-step process for conversion of Ume6 from a transcriptional repressor to an activator in yeast, *Mol Cell Biol 21*, 2057-2069.

[53] Mews, P., Donahue, G., Drake, A. M., Luczak, V., Abel, T., and Berger, S. L. (2017) Acetyl-CoA synthetase regulates histone acetylation and hippocampal memory, *Nature 546*, 381-386.

[54] Barrios, A., Selleck, W., Hnatkovich, B., Kramer, R., Sermwittayawong, D., and Tan, S. (2007) Expression and purification of recombinant yeast Ada2/Ada3/Gcn5 and Piccolo NuA4 histone acetyltransferase complexes, *Methods 41*, 271-277.

[55] Liu, H., and Naismith, J. H. (2008) An efficient one-step site-directed deletion, insertion, single and multiple-site plasmid mutagenesis protocol, *BMC Biotechnol 8*, 91.

[56] Todd, A. P., Cong, J., Levinthal, F., Levinthal, C., and Hubbell, W. L. (1989) Site-directed mutagenesis of colicin E1 provides specific attachment sites for spin labels whose spectra are sensitive to local conformation, *Proteins 6*, 294-305.

[57] Laughery, M. F., Hunter, T., Brown, A., Hoopes, J., Ostbye, T., Shumaker, T., and Wyrick, J. J. (2015) New vectors for simple and streamlined CRISPR-Cas9 genome editing in Saccharomyces cerevisiae, *Yeast 32*, 711-720.

[58] Labun, K., Montague, T. G., Gagnon, J. A., Thyme, S. B., and Valen, E. (2016) CHOPCHOP v2: a web tool for the next generation of CRISPR genome engineering, *Nucleic Acids Res 44*, W272-276.

[59] Labun, K., Montague, T. G., Krause, M., Torres Cleuren, Y. N., Tjeldnes, H., and Valen, E. (2019) CHOPCHOP v3: expanding the CRISPR web toolbox beyond genome editing, *Nucleic Acids Res 47*, W171-W174.

[60] Montague, T. G., Cruz, J. M., Gagnon, J. A., Church, G. M., and Valen, E. (2014) CHOPCHOP: a CRISPR/Cas9 and TALEN web tool for genome editing, *Nucleic Acids Res 42*, W401-407.

[61] FlowJo Software (2023 for Mac) Version 10.9.0. Ashland, B., Dickinson, and Company. FlowJo Software (2023 for Mac) Version 10.9.0. Ashland, Becton, Dickinson, and Company.
[62] Schneider, C. A., Rasband, W. S., and Eliceiri, K. W. (2012) NIH Image to ImageJ: 25 years of image analysis, *Nat Methods 9*, 671-675.
[63] Schindelin, J., Arganda-Carreras, I., Frise, E., Kaynig, V., Longair, M., Pietzsch, T., Preibisch, S., Rueden, C., Saalfeld, S., Schmid, B., Tinevez, J. Y., White, D. J., Hartenstein, V., Eliceiri, K., Tomancak, P., and Cardona, A. (2012) Fiji: an open-source platform for biological-image analysis, *Nat Methods 9*, 676-682.
[64] Teste, M. A., Duquenne, M., Francois, J. M., and Parrou, J. L. (2009) Validation of reference genes for quantitative expression analysis by real-time RT-PCR in Saccharomyces cerevisiae, *BMC Mol Biol 10*, 99.
[65] Nadai, C., Campanaro, S., Giacomini, A., and Corich, V. (2015) Selection and validation of reference genes for quantitative real-time PCR studies during Saccharomyces cerevisiae alcoholic fermentation in the presence of sulfite, *Int J Food Microbiol 215*, 49-56.
[66] Paul, S., Singh, S., Chakrabarti, A., Rudramurthy, S. M., and Ghosh, A. K. (2020) Selection and evaluation of appropriate reference genes for RT-qPCR based expression analysis in Candida tropicalis following azole treatment, *Sci Rep 10*, 1972.

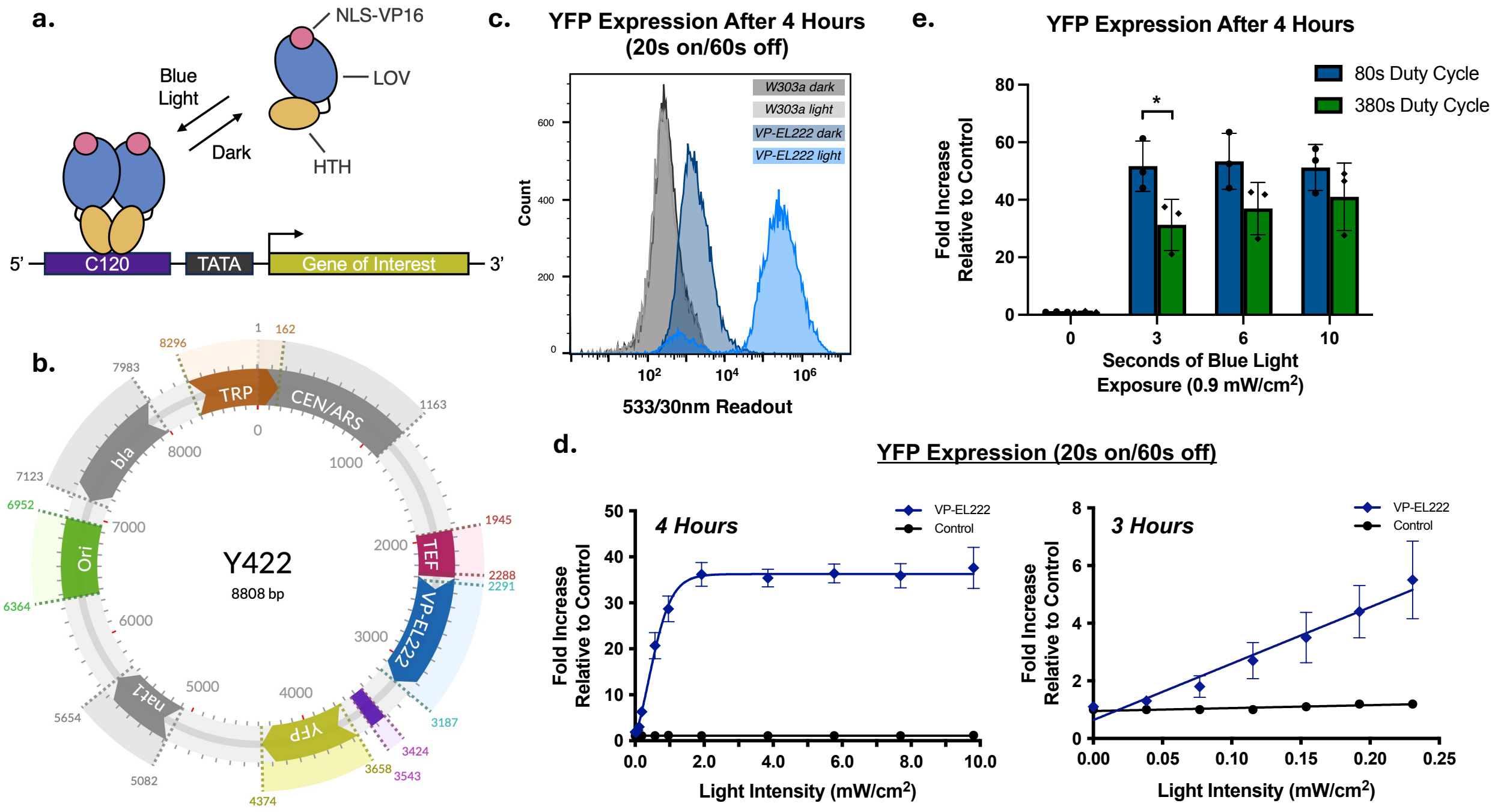
a.
NLS-VP16
LOV
HTH
Blue Light
Dark
5'
C120
TATA
Gene of Interest
3'
b.
Y422
8808 bp
TRP
CEN/ARS
bla
Ori
TEF
VP-EL222
YFP
natr1
1
162
1163
1945
2288
2291
3187
3424
3543
3658
4374
5082
5654
6364
6952
7123
7983
8296
0
1000
2000
3000
4000
5000
6000
7000
8000
c.
YFP Expression After 4 Hours
(20s on/60s off)
W303a dark
W303a light
VP-EL222 dark
VP-EL222 light
Count
533/30nm Readout
d.
YFP Expression (20s on/60s off)
4 Hours
3 Hours
VP-EL222
Control
Fold Increase Relative to Control
Light Intensity (mW/cm2)
e.
YFP Expression After 4 Hours
80s Duty Cycle
380s Duty Cycle
Fold Increase Relative to Control
Seconds of Blue Light Exposure (0.9 mW/cm2)

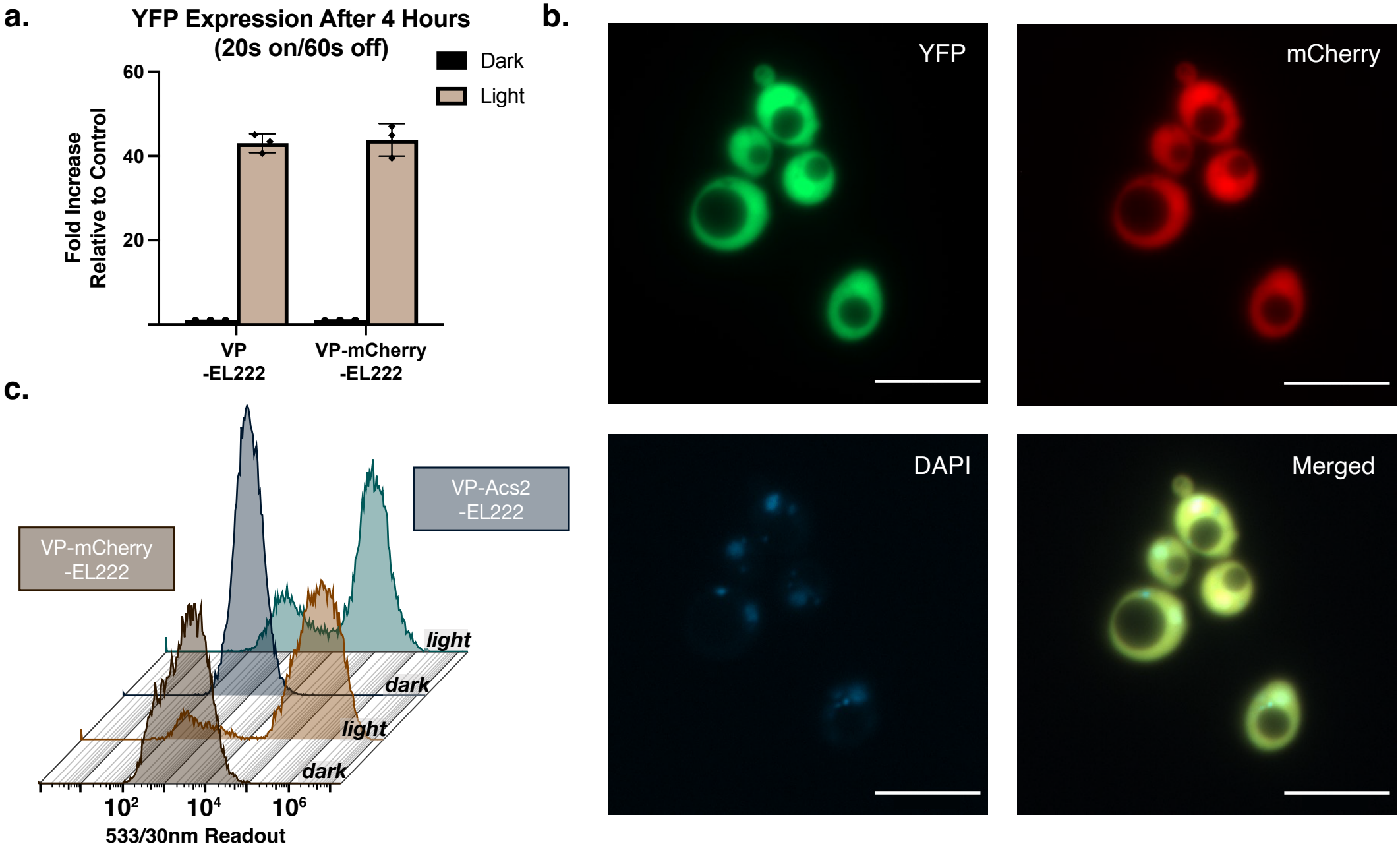
a.
YFP Expression After 4 Hours
(20s on/60s off)
Dark
Light
Fold Increase
Relative to Control
60
40
20
VP
-EL222
VP-mCherry
-EL222
b.
YFP
mCherry
DAPI
Merged
c.
VP-Acs2
-EL222
VP-mCherry
-EL222
light
dark
light
dark
10^2
10^4
10^6
533/30nm Readout

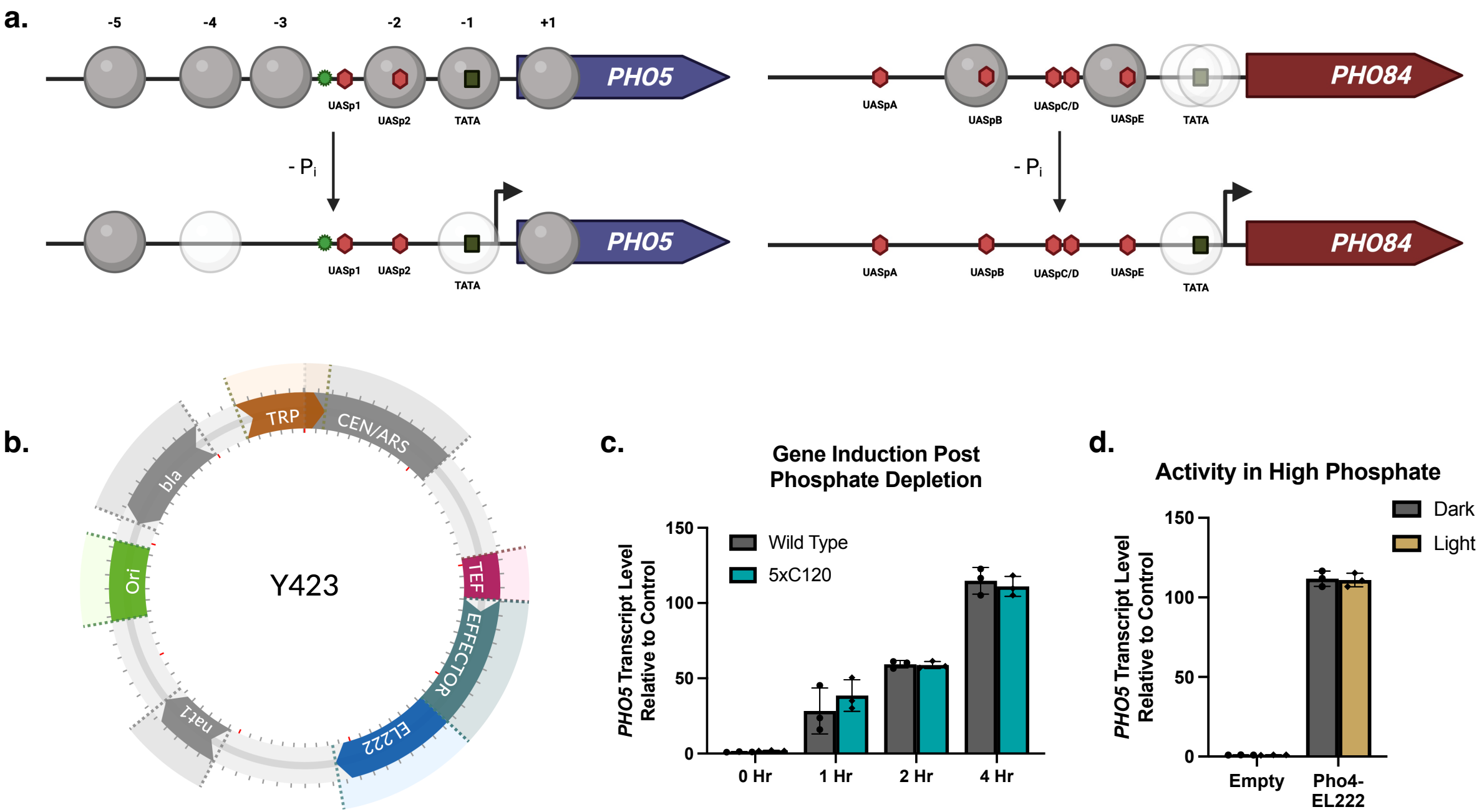
a.
-5
-4
-3
-2
-1
+1
PHO5
UASp1
UASp2
TATA
- Pi
PHO84
UASpA
UASpB
UASpC/D
UASpE
b.
TRP
CEN/ARS
bla
Ori
Y423
TEF
EFFECTOR
EL222
natr1
c.
Gene Induction Post Phosphate Depletion
PHO5 Transcript Level Relative to Control
Wild Type
5xC120
0 Hr
1 Hr
2 Hr
4 Hr
d.
Activity in High Phosphate
Dark
Light
Empty
Pho4-EL222

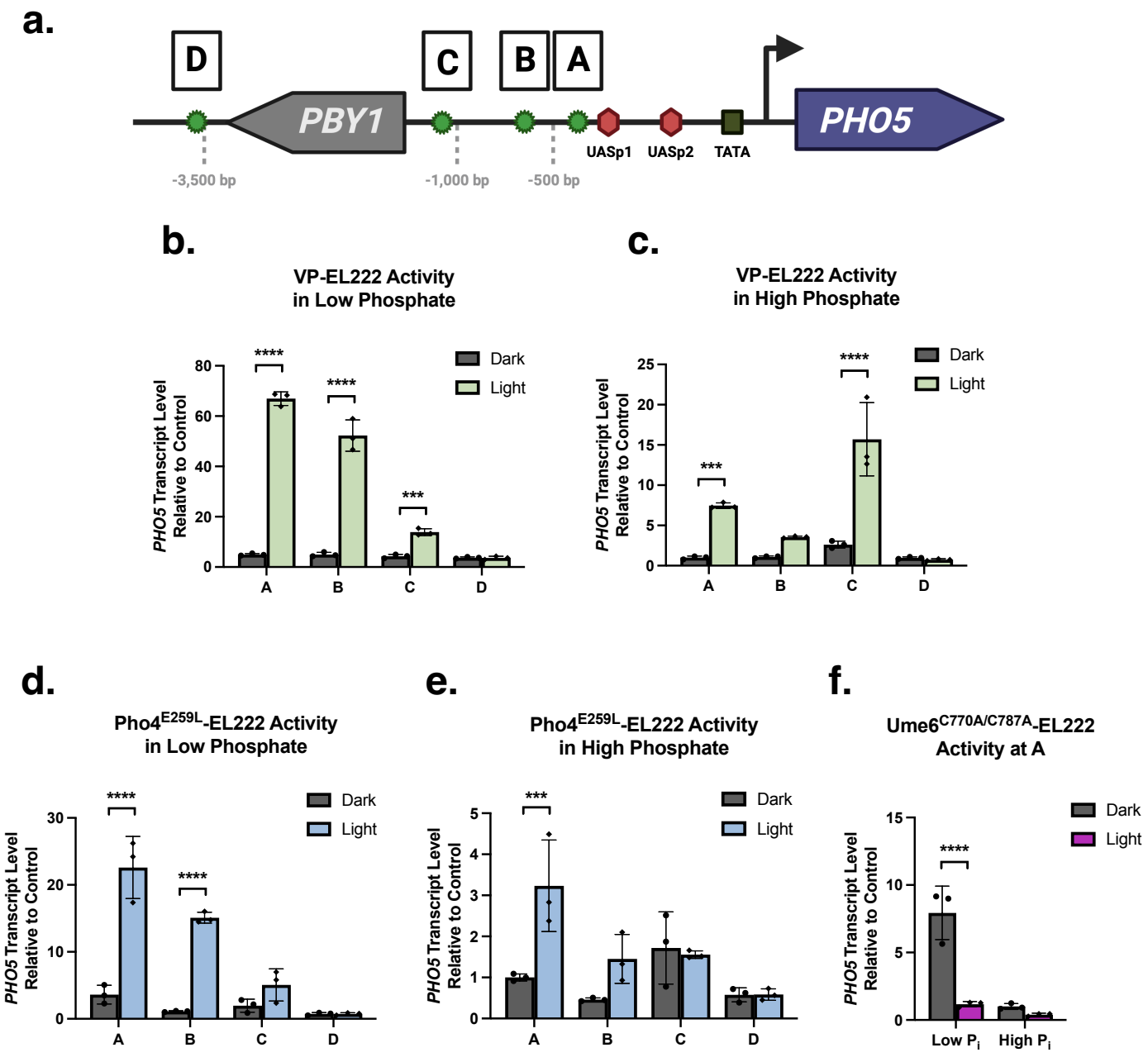
a.
D
C
B
A
PBY1
PHO5
UASp1
UASp2
TATA
-3,500 bp
-1,000 bp
-500 bp
b.
VP-EL222 Activity
in Low Phosphate
PHO5 Transcript Level
Relative to Control
Dark
Light
A
B
C
D
c.
VP-EL222 Activity
in High Phosphate
d.
Pho4E259L-EL222 Activity
in Low Phosphate
e.
Pho4E259L-EL222 Activity
in High Phosphate
f.
Ume6C770A/C787A-EL222
Activity at A
Low Pi
High Pi

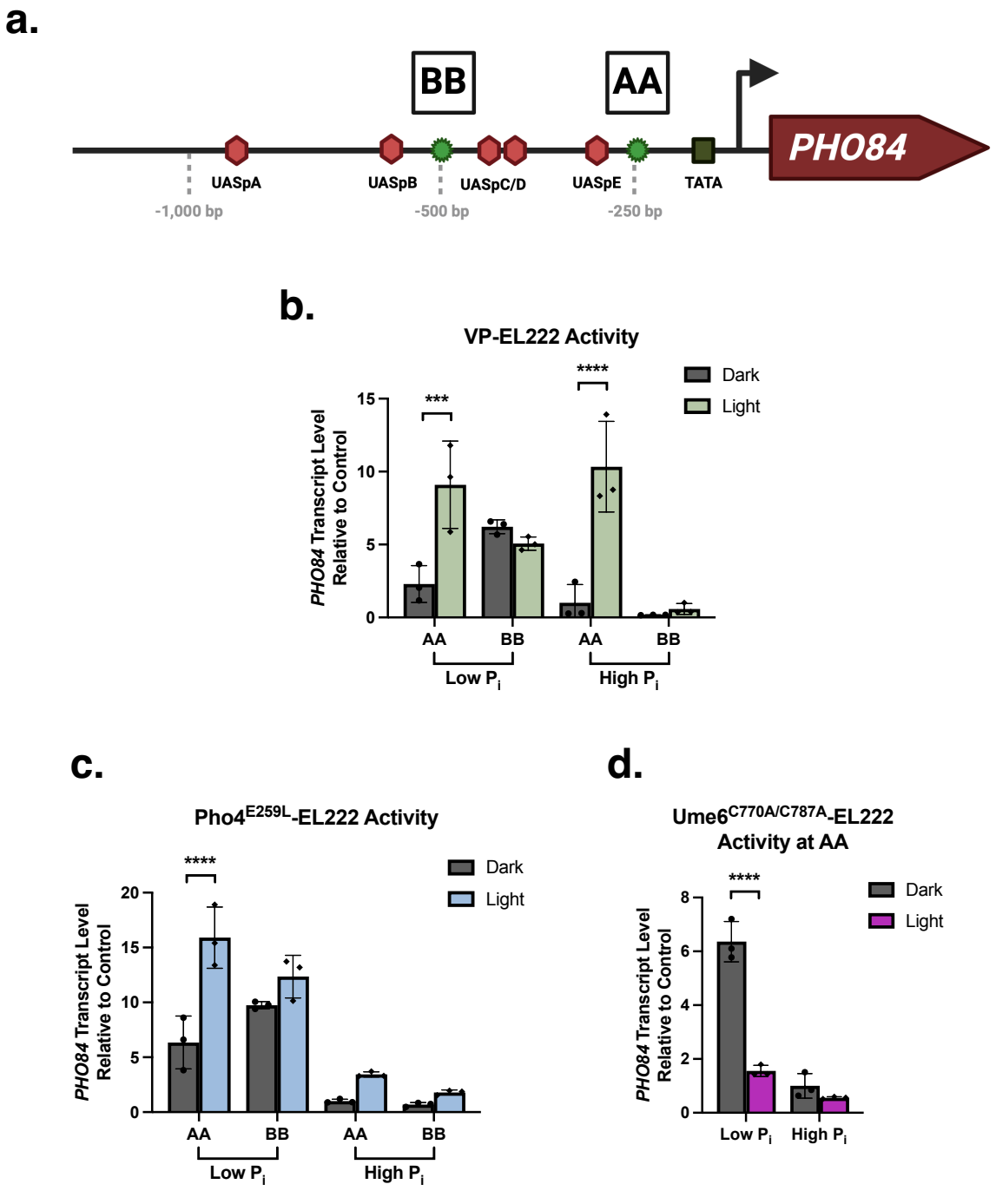
a.
BB
AA
PHO84
UASpA
UASpB
UASpC/D
UASpE
TATA
-1,000 bp
-500 bp
-250 bp
b.
VP-EL222 Activity
Dark
Light
PHO84 Transcript Level Relative to Control
***
****
AA
BB
AA
BB
Low Pi
High Pi
c.
Pho4E259L-EL222 Activity
Dark
Light
PHO84 Transcript Level Relative to Control
****
AA
BB
AA
BB
Low Pi
High Pi
d.
Ume6C770A/C787A-EL222 Activity at AA
Dark
Light
PHO84 Transcript Level Relative to Control
****
Low Pi
High Pi